On the Handling Dynamics of Automated Vehicles: An Appellian View

Gábor Orosz, Illés Vörös, and Dénes Takács

Abstract Single track models of automobiles are constructed by using the Appellian approach that provides the equations of motions in the most simplistic form in the presence of kinematic constraints. Models with rigid wheels and elastic tires are derived, and their behaviors are compared in steady state as well as in transient maneuvers.

1 Introduction

Vehicle dynamics started to develop in the 1950s (Segel, 1956) when automobiles reached speeds where their dynamical properties demanded attention. As the field matured the arising knowledge was collected into books by many prominent scientists and engineers (Gillespie, 1992; Pacejka, 2002; Popp and Schiehlen, 2010; Rajamani, 2012; Schramm et al., 2014; Ulsoy et al., 2012). The equations of motion were typically constructed following the Newtonian/Eulerian approach (Euler, 1736; Newton, 1687), which requires one to eliminate the constraining forces acting between bodies. However, this approach does not scale well once the number of bodies increases, and a recent trend in the literature is to utilize other, more advanced, approaches from analytical mechanics (Limebeer and Massaro, 2018).

Following this trend, we utilize methods from nonholonomic mechanical systems to handle kinematic constraints that depend on velocities. Nonholonomic mechanics has a long history (Appell, 1900; Baruh, 1999; Bloch, 2003; De Sapio, 2017; Gantmacher, 1970; Gibbs, 1879; Greenwood, 2003; Hamel, 1938; Kane, 1961; Kane and

G. Orosz · I. Vörös
Department of Mechanical Engineering, University of Michigan, Ann Arbor, MI, USA

G. Orosz (✉)
Department of Civil and Environmental Engineering, University of Michigan, Ann Arbor, MI, USA
e-mail: orosz@umich.edu

I. Vörös · D. Takács
Department of Applied Mechanics, Budapest University of Technology and Economics, Budapest, Hungary

B. Lenzo and F. Naets (eds.), *Vehicle Dynamics, Control and Design*, CISM International Centre for Mechanical Sciences 620, https://doi.org/10.1007/978-3-031-97270-6_5

Levinson, 1985; Koon and Marsden, 1997; Neimark and Fufaev, 1972; Ostrovskaya and Angeles, 1998; Papastavridis, 2002; Routh, 1884; Voss, 1885; Voronets, 1901) but the results mostly stayed in academia and did not penetrate the industry. This is in contrast with holonomic mechanics, which deals with geometric constraints that depend on the coordinates only. For example, the Lagrangian approach (Lagrange, 1788), which can eliminate geometric constraints with the appropriate selection of generalized (configuration) coordinates, deeply penetrated the field of robotics. This approach delivers second order differential equations, as many as degrees of freedom the system has.

In nonholonomic systems, a major challenge is that the constraints are formulated as first order differential equations, and these cannot be fully eliminated but have to be carried forward. That is, while adding a geometric constraint reduces the number of degrees of freedom by one, adding a kinematic constraint only reduces it by half. One shall select so-called pseudo velocities (as many as the number of configuration coordinates minus the number of kinematic constraints). Then by constructing the Appell–Gibbs equations (Appell, 1900; Gibbs, 1879) or the Kane equations (Kane, 1961), it is possible to derive first order differential equations, whose number is two times the number of configuration coordinates minus the number of kinematic constraints. Indeed this may be an odd number resulting in half degrees of freedom when divided by two. In this book chapter, we follow this approach and refer to it as the Appellian approach.

Our goal is to demonstrate the applicability of the Appellian approach to vehicle dynamics. As rolling without slipping can be formulated as kinematic constraints, the approach was first proven to be successful when considering vehicles with rigid wheels (Qin et al., 2022; Várszegi et al., 2019). Here we also start with such simplified models as these already capture some essential parts of vehicle dynamics. However, kinematic constraints (like maintaining constant longitudinal velocity) can still be imposed when considering vehicles with elastic tires (Beregi et al., 2023; Oh et al., 2021; Vörös and Takács, 2022; Vörös et al., 2023a, b). Then, with the appropriate choice of pseudo velocities, the Appellian approach delivers the most simplistic form of the equations of motion.

This approach particularly shines when considering multibody representations of the vehicles, e.g., by adding the steering dynamics to the vehicle dynamics as demonstrated in this paper. One may also add the longitudinal and/or wheel speed dynamics as in Goh et al. (2020), Goh et al. (2024), Lenzo et al. (2024), Mastinu et al. (2023), Peterson et al. (2023), Steindl et al. (2023), Weber and Gerdes (2024), but this is beyond the scope of this book chapter. The constructed models facilitate a multitude of control design and may allow one to study effects like time delays in the control loop (Beregi et al., 2023; Lu et al., 2022; Vörös and Takács, 2022; Vörös et al., 2023a, b). These are also omitted here in order to limit the scope of the book chapter.

The layout of this chapter is as follows. In Sect. 2, we construct single track vehicle models without and with steering dynamics while considering rigid wheels. In Sect. 3, we derive tire models for elastic tires while we integrate these with single

track vehicle models in Sect. 4. A detailed description of the Appellian approach is presented in Appendix 6. For readers who are not familiar with this approach, it is recommended to start with this Appendix.

2 Vehicle Models with Rigid Wheels

In this section, we omit the elasticity of the tires and consider vehicles with rigid wheels. While this is clearly an approximation, it provides a simplistic description of vehicle dynamics and allows one to describe the fundamentals of vehicle motions. The models developed here will be augmented with tire models in later sections of this chapter.

In Fig. 1, the dimmed part shows the top view of a four-wheeled, front-wheel-steered vehicle. By approximating the front wheel pair with a single front wheel and the rear wheel pair with a single rear wheel, we obtain an abstraction of the vehicle, called the single track model or bicycle model (Gillespie, 1992; Limebeer and Massaro, 2018; Popp and Schiehlen, 2010; Rajamani, 2012; Schramm et al., 2014; Ulsoy et al., 2012), which is emphasized by dark gray color. The mass of the vehicle body is m, the wheelbase is l, the distance between the rear axle and the center of mass G is d, and the mass moment of inertia of the vehicle body about the vertical axis at the center of mass G is J_G. Points R and F mark the centers of the rear and front wheels, respectively.

We define multiple (right-hand) coordinate systems as follows.

1. (x_0, y_0, z_0) is the Earth-fixed frame (denoted as $\mathcal{F}_0$);
2. (x_1, y_1, z_1) is a frame fixed to the vehicle body (denoted as $\mathcal{F}_1$) with the origin located at the center of the rear wheel R, the x_1 and y_1 axes pointing towards the longitudinal and lateral directions;

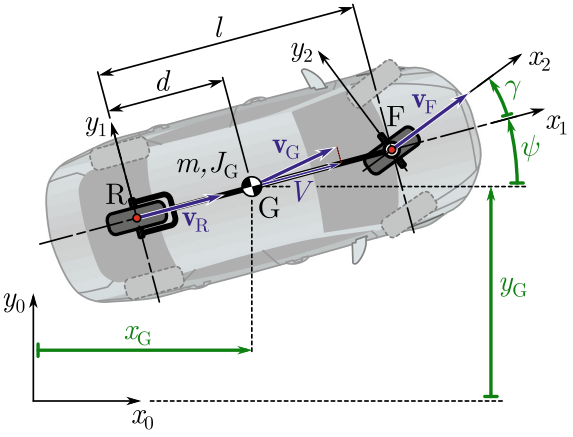

Fig. 1 Single track model (also called bicycle model) of an automobile with rigid wheels. The geometry, coordinate frames and kinematics are indicated

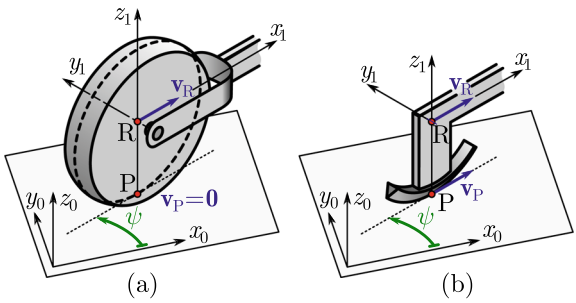

Fig. 2 Models of rigid rolling wheel (**a**) and skate (**b**) with geometry and kinematics indicated

3. (x_2, y_2, z_2) is a frame fixed to the front wheel (denoted as $\mathcal{F}_2$) with the origin located at the center of the front wheel F, the x_2 and y_2 axes pointing towards the longitudinal and lateral directions of the front wheel.

In the Earth-fixed frame $\mathcal{F}_0$, the positions of points G, R and F are (x_G, y_G), (x_R, y_R) and (x_F, y_F), respectively. The yaw angle of the vehicle is ψ, the steering angle is denoted as γ.

In this section, we consider a single contact point at each wheel with no-slip condition; see De Luca et al. (1998), Qin et al. (2022), Várszegi et al. (2019). This approach can be formulated by the consideration of a *rigid wheel* or a *skate*. Both cases result in kinematic constraints such that velocity vectors of the wheel centers align with the wheel planes as illustrated in Fig. 2. For simplicity, the masses and mass moments of inertia of the wheels are neglected, with the exception of the mass moment of inertia of the front wheel about the vertical axis, denoted as J_F, which is equivalent to the overall rotational inertia of the steering system when the vehicle is steered by applying the steering torque T_s. Note that, however, the forms of the equations do not change once the other wheel masses and mass moments of inertia are incorporated; see Qin et al. (2022).

In the following two subsections, we describe vehicle models when the steering angle is prescribed and when the vehicle is steered by a steering torque.

2.1 Kinematic Bicycle Model

Since the vehicle is moving in two-dimensional space, three generalized coordinates are needed to describe its position and orientation. Here we choose the position (x_G, y_G) of the center of mass G and the yaw angle ψ. Alternatively, one may choose the position (x_R, y_R) of the center of the rear axle R and the yaw angle ψ as will be discussed further below.

The position vectors of points G, R and F are given in frame $\mathcal{F}_0$ as

$$\begin{aligned}
\mathbf{r}_{\mathrm{G}} &= \begin{bmatrix} x_{\mathrm{G}} \\ y_{\mathrm{G}} \end{bmatrix}_{\mathcal{F}_0}, \\
\mathbf{r}_{\mathrm{R}} &= \begin{bmatrix} x_{\mathrm{R}} \\ y_{\mathrm{R}} \end{bmatrix}_{\mathcal{F}_0} = \begin{bmatrix} x_{\mathrm{G}} - d\cos\psi \\ y_{\mathrm{G}} - d\sin\psi \end{bmatrix}_{\mathcal{F}_0}, \\
\mathbf{r}_{\mathrm{F}} &= \begin{bmatrix} x_{\mathrm{F}} \\ y_{\mathrm{F}} \end{bmatrix}_{\mathcal{F}_0} = \begin{bmatrix} x_{\mathrm{G}} + (l-d)\cos\psi \\ y_{\mathrm{G}} + (l-d)\sin\psi \end{bmatrix}_{\mathcal{F}_0}.
\end{aligned} \tag{1}$$

The velocities, i.e., first derivatives with respect to time are given by

$$\begin{aligned}
\mathbf{v}_{\mathrm{G}} &= \dot{\mathbf{r}}_{\mathrm{G}} = \begin{bmatrix} \dot{x}_{\mathrm{G}} \\ \dot{y}_{\mathrm{G}} \end{bmatrix}_{\mathcal{F}_0}, \\
\mathbf{v}_{\mathrm{R}} &= \dot{\mathbf{r}}_{\mathrm{R}} = \begin{bmatrix} \dot{x}_{\mathrm{R}} \\ \dot{y}_{\mathrm{R}} \end{bmatrix}_{\mathcal{F}_0} = \begin{bmatrix} \dot{x}_{\mathrm{G}} + d\,\dot{\psi}\sin\psi \\ \dot{y}_{\mathrm{G}} - d\,\dot{\psi}\cos\psi \end{bmatrix}_{\mathcal{F}_0}, \\
\mathbf{v}_{\mathrm{F}} &= \dot{\mathbf{r}}_{\mathrm{F}} = \begin{bmatrix} \dot{x}_{\mathrm{F}} \\ \dot{y}_{\mathrm{F}} \end{bmatrix}_{\mathcal{F}_0} = \begin{bmatrix} \dot{x}_{\mathrm{G}} - (l-d)\,\dot{\psi}\sin\psi \\ \dot{y}_{\mathrm{G}} + (l-d)\,\dot{\psi}\cos\psi \end{bmatrix}_{\mathcal{F}_0},
\end{aligned} \tag{2}$$

while accelerations, i.e., the second derivatives, read

$$\begin{aligned}
\mathbf{a}_{\mathrm{G}} &= \ddot{\mathbf{r}}_{\mathrm{G}} = \begin{bmatrix} \ddot{x}_{\mathrm{G}} \\ \ddot{y}_{\mathrm{G}} \end{bmatrix}_{\mathcal{F}_0}, \\
\mathbf{a}_{\mathrm{R}} &= \ddot{\mathbf{r}}_{\mathrm{R}} = \begin{bmatrix} \ddot{x}_{\mathrm{R}} \\ \ddot{y}_{\mathrm{R}} \end{bmatrix}_{\mathcal{F}_0} = \begin{bmatrix} \ddot{x}_{\mathrm{G}} + d\,\ddot{\psi}\sin\psi + d\,\dot{\psi}^2\cos\psi \\ \ddot{y}_{\mathrm{G}} - d\,\ddot{\psi}\cos\psi + d\,\dot{\psi}^2\sin\psi \end{bmatrix}_{\mathcal{F}_0}, \\
\mathbf{a}_{\mathrm{F}} &= \ddot{\mathbf{r}}_{\mathrm{F}} = \begin{bmatrix} \ddot{x}_{\mathrm{F}} \\ \ddot{y}_{\mathrm{F}} \end{bmatrix}_{\mathcal{F}_0} = \begin{bmatrix} \ddot{x}_{\mathrm{G}} - (l-d)\,\ddot{\psi}\sin\psi - (l-d)\,\dot{\psi}^2\cos\psi \\ \ddot{y}_{\mathrm{G}} + (l-d)\,\ddot{\psi}\cos\psi - (l-d)\,\dot{\psi}^2\sin\psi \end{bmatrix}_{\mathcal{F}_0}.
\end{aligned} \tag{3}$$

Note that the third components of the vectors in (1)–(3) are zeros and these are not spelled out for brevity. This convention is followed in the rest of this book chapter.

Without any kinematic constraints, the vehicle body would have three degrees of freedom, i.e., three second order ordinary differential equations would describe the motion. Below, we will show how the number of degrees of freedom, i.e., the number of ordinary differential equations, will be reduced due to the kinematic constraints. Here we assume that the steering angle γ is prescribed. Thus it does not lead to an additional degree of freedom but rather acts as an input to the system.

The kinematic constraints of the rigid wheels/skates result in that the velocities of the wheel center points align with the wheel planes, that is, the lateral velocity components of the points R and F, i.e., the velocity components that are perpendicular to the wheels, are zero:

$$v_{\mathrm{R}}^{y_1} = 0, \quad v_{\mathrm{F}}^{y_2} = 0. \tag{4}$$

The velocities of points G, R and F can be expressed in the frame $\mathcal{F}_1$ as

$$\begin{aligned}
\mathbf{v}_\mathrm{G} &= \begin{bmatrix} \dot{x}_\mathrm{G}\cos\psi + \dot{y}_\mathrm{G}\sin\psi \\ -\dot{x}_\mathrm{G}\sin\psi + \dot{y}_\mathrm{G}\cos\psi \end{bmatrix}_{\mathcal{F}_1}, \\
\mathbf{v}_\mathrm{R} &= \begin{bmatrix} \dot{x}_\mathrm{R}\cos\psi + \dot{y}_\mathrm{R}\sin\psi \\ -\dot{x}_\mathrm{R}\sin\psi + \dot{y}_\mathrm{R}\cos\psi \end{bmatrix}_{\mathcal{F}_1} = \begin{bmatrix} \dot{x}_\mathrm{G}\cos\psi + \dot{y}_\mathrm{G}\sin\psi \\ -\dot{x}_\mathrm{G}\sin\psi + \dot{y}_\mathrm{G}\cos\psi - d\dot{\psi} \end{bmatrix}_{\mathcal{F}_1}, \\
\mathbf{v}_\mathrm{F} &= \begin{bmatrix} \dot{x}_\mathrm{F}\cos\psi + \dot{y}_\mathrm{F}\sin\psi \\ -\dot{x}_\mathrm{F}\sin\psi + \dot{y}_\mathrm{F}\cos\psi \end{bmatrix}_{\mathcal{F}_1} = \begin{bmatrix} \dot{x}_\mathrm{G}\cos\psi + \dot{y}_\mathrm{G}\sin\psi \\ -\dot{x}_\mathrm{G}\sin\psi + \dot{y}_\mathrm{G}\cos\psi + (l-d)\dot{\psi} \end{bmatrix}_{\mathcal{F}_1},
\end{aligned} \tag{5}$$

respectively. These vectors can also be represented in the frame $\mathcal{F}_2$ but here we only spell out the velocity of point F

$$\begin{aligned}
\mathbf{v}_\mathrm{F} &= \begin{bmatrix} \dot{x}_\mathrm{F}\cos(\psi+\gamma) + \dot{y}_\mathrm{F}\sin(\psi+\gamma) \\ -\dot{x}_\mathrm{F}\sin(\psi+\gamma) + \dot{y}_\mathrm{F}\cos(\psi+\gamma) \end{bmatrix}_{\mathcal{F}_2} \\
&= \begin{bmatrix} \dot{x}_\mathrm{G}\cos(\psi+\gamma) + \dot{y}_\mathrm{G}\sin(\psi+\gamma) + (l-d)\dot{\psi}\,\sin\gamma \\ -\dot{x}_\mathrm{G}\sin(\psi+\gamma) + \dot{y}_\mathrm{G}\cos(\psi+\gamma) + (l-d)\dot{\psi}\,\cos\gamma \end{bmatrix}_{\mathcal{F}_2}.
\end{aligned} \tag{6}$$

Substituting (5) and (6) into (4) results in the constraining equations

$$\begin{aligned}
&-\dot{x}_\mathrm{G}\sin\psi + \dot{y}_\mathrm{G}\cos\psi - d\,\dot{\psi} = 0, \\
&-\dot{x}_\mathrm{G}\sin(\psi+\gamma) + \dot{y}_\mathrm{G}\cos(\psi+\gamma) + (l-d)\dot{\psi}\,\cos\gamma = 0.
\end{aligned} \tag{7}$$

In the simplest model we assume that, beside the steering angle γ, the longitudinal velocity is also prescribed, that is,

$$v_\mathrm{G}^{x_1} = v_\mathrm{R}^{x_1} = v_\mathrm{F}^{x_1} = V. \tag{8}$$

By using (5) we obtain the kinematic constraint

$$\dot{x}_\mathrm{G}\cos\psi + \dot{y}_\mathrm{G}\sin\psi = V\,. \tag{9}$$

For simplicity, we assume that V is constant and this assumption is kept for all models presented in this paper. The three kinematic constraints given by (7) and (9) result in $3 - 3\frac{1}{2} = 1.5$ degrees of freedom, that is, the system can be described by three first order differential equations. In fact, the number of pseudo velocities needed is $3 - 3 = 0$ and the kinematic constraints themselves describe the system unambiguously (see Appendix 6 for more details on concepts related to nonholonomic systems). Solving (7), (9) for the generalized velocities we obtain the equation of motion:

$$\begin{aligned} \dot{x}_{\mathrm{G}} &= V\Big(\cos\psi - \frac{d}{l}\sin\psi\tan\gamma\Big), \\ \dot{y}_{\mathrm{G}} &= V\Big(\sin\psi + \frac{d}{l}\cos\psi\tan\gamma\Big), \\ \dot{\psi} &= \frac{V}{l}\tan\gamma. \end{aligned} \tag{10}$$

Following through the same process while using the position coordinates $(x_{\mathrm{R}}, y_{\mathrm{R}})$ of the rear axle center point R as generalized coordinates, one may obtain the kinematic constraining equations

$$\begin{aligned} &-\dot{x}_{\mathrm{R}}\sin\psi + \dot{y}_{\mathrm{R}}\cos\psi = 0, \\ &-\dot{x}_{\mathrm{R}}\sin(\psi+\gamma) + \dot{y}_{\mathrm{R}}\cos(\psi+\gamma) + l\dot{\psi}\cos\gamma = 0, \end{aligned} \tag{11}$$

instead of (7) and

$$\dot{x}_{\mathrm{R}}\cos\psi + \dot{y}_{\mathrm{R}}\sin\psi = V\,, \tag{12}$$

instead of (9). Solving these results in the equations of motion

$$\begin{aligned} \dot{x}_{\mathrm{R}} &= V\cos\psi, \\ \dot{y}_{\mathrm{R}} &= V\sin\psi, \\ \dot{\psi} &= \frac{V}{l}\tan\gamma. \end{aligned} \tag{13}$$

We will show below that such re-writing can also be utilized for more complicated single track models.

As the Appellian approach eliminates the kinematic constraints, one needs to use the Newtonian approach to calculate the corresponding constraining forces. As illustrated in Fig. 3, the three constraining forces F_{R}, F_{F} and R correspond to the constraints (7) and (9). That is, the lateral forces F_{R}, F_{F} ensure the no-sideslip

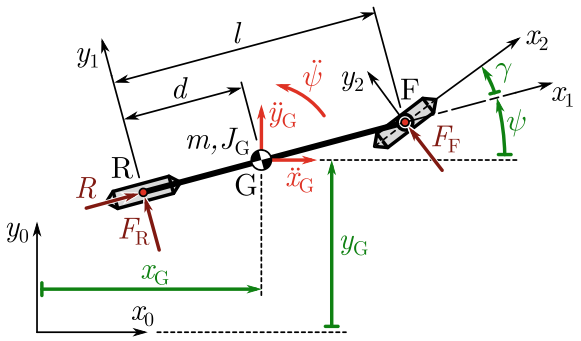

Fig. 3 Free body diagram of the vehicle body when the steering angle and the longitudinal speed are prescribed. The constraining forces acting at the vehicle body are shown

constraints at the front and rear wheels, respectively, while the propulsion force R maintains the constant longitudinal velocity. The resulting Newton equations are given in the frame $\mathcal{F}_1$:

$$\begin{aligned} m(\ddot{x}_G \cos\psi + \ddot{y}_G \sin\psi) &= R - F_F \sin\gamma, \\ m(-\ddot{x}_G \sin\psi + \ddot{y}_G \cos\psi) &= F_R + F_F \cos\gamma, \\ J_G \ddot{\psi} &= -d\, F_R + (l-d) F_F \cos\gamma. \end{aligned} \tag{14}$$

Taking the time derivative of (10) results in

$$\begin{aligned} \ddot{x}_G &= -\frac{V^2}{l}\tan\gamma\left(\sin\psi + \frac{d}{l}\cos\psi\tan\gamma\right) - \frac{dV}{l}\frac{\sin\psi}{\cos^2\gamma}\dot{\gamma}, \\ \ddot{y}_G &= \frac{V^2}{l}\tan\gamma\left(\cos\psi - \frac{d}{l}\sin\psi\tan\gamma\right) + \frac{dV}{l}\frac{\cos\psi}{\cos^2\gamma}\dot{\gamma}, \\ \ddot{\psi} &= \frac{V}{l\cos^2\gamma}\dot{\gamma}. \end{aligned} \tag{15}$$

Substituting this into (14) yields the constraining forces

$$\begin{aligned} F_R &= \frac{V}{l^2}\left(m(l-d)V\tan\gamma - \left(J_G + md^2 - mld\right)\frac{\dot{\gamma}}{\cos^2\gamma}\right), \\ F_F &= \frac{V}{l^2\cos^3\gamma}\left(mdV\sin\gamma\cos\gamma + \left(J_G + md^2\right)\dot{\gamma}\right), \\ R &= \frac{V\sin\gamma}{l^2\cos^3\gamma}\left(J_G + md^2\right)\dot{\gamma}. \end{aligned} \tag{16}$$

Observe that for steady state cornering $\gamma(t) \equiv \gamma_* \Rightarrow \dot{\gamma}(t) \equiv 0$ some of the terms become zero, in particular we obtain $R = 0$ since the longitudinal resistance terms are neglected in the model.

Finally, we remark that conditions (9) and (12) strictly speaking mean that the speed of the rear wheel center R is constant, which can be ensured for a rear wheel drive (RWD) vehicle using cruise control. For front wheel drive vehicles (FWD), on the other hand, one may rather control the speed of the front wheel center F. That is, (9) should be substituted with

$$\dot{x}_G \cos(\psi+\gamma) + \dot{y}_G \sin(\psi+\gamma) + (l-d)\dot{\psi}\sin\gamma = \hat{V}, \tag{17}$$

which should be combined with (7) to obtain the equations of motion. Similarly, when using the coordinates of the rear axle center R, (12) should be substituted with

$$\dot{x}_R \cos(\psi+\gamma) + \dot{y}_R \sin(\psi+\gamma) + l\dot{\psi}\sin\gamma = \hat{V}, \tag{18}$$

which should be combined with (11) to obtain the equations of motion. These calculations are omitted here for brevity, but the reader is encouraged to try to derive these models.

2.1.1 Steady State Cornering

The steady state cornering motion of (10) and (13) can be obtained by substituting $\gamma(t) \equiv \gamma_*$. Then defining the steady state yaw rate

$$\omega_* := \frac{V}{l} \tan \gamma_* \,, \tag{19}$$

and integrating the equations yields

$$\begin{aligned} \psi(t) &= \omega_* t + \psi_0, \\ x_{\mathrm{G}}(t) &= \frac{V}{\omega_*} \sin(\omega_* t + \psi_0) + d \cos(\omega_* t + \psi_0) + x_{\mathrm{C}}, \\ y_{\mathrm{G}}(t) &= -\frac{V}{\omega_*} \cos(\omega_* t + \psi_0) + d \sin(\omega_* t + \psi_0) + y_{\mathrm{C}}, \end{aligned} \tag{20}$$

and

$$\begin{aligned} \psi(t) &= \omega_* t + \psi_0, \\ x_{\mathrm{R}}(t) &= \frac{V}{\omega_*} \sin(\omega_* t + \psi_0) + x_{\mathrm{C}}, \\ y_{\mathrm{R}}(t) &= -\frac{V}{\omega_*} \cos(\omega_* t + \psi_0) + y_{\mathrm{C}}, \end{aligned} \tag{21}$$

where $\psi_0 = \psi(0)$ while x_{C} and y_{C} also come from the initial conditions.

These formulae describe the circular motion of the vehicle where $(x_{\mathrm{C}}, y_{\mathrm{C}})$ are the coordinates of the position of the instantaneous center of rotation as shown in Fig. 4. Using (20) and (21), one may show that $(x_{\mathrm{G}} - x_{\mathrm{R}})^2 + (y_{\mathrm{G}} - y_{\mathrm{R}})^2 = d^2$, which justifies why the constants x_{C} and y_{C} need to be the same in both formulae. The radius of curvature for the center of mass G and for the rear axle center R can be calculated as

$$\rho_{\mathrm{G}} = \sqrt{(x_{\mathrm{G}} - x_{\mathrm{C}})^2 + (y_{\mathrm{G}} - y_{\mathrm{C}})^2} = \frac{\sqrt{V^2 + d^2 \omega_*^2}}{|\omega_*|} = \sqrt{\frac{l^2}{\tan^2 \gamma_*} + d^2}, \tag{22}$$

and

$$\rho_{\mathrm{R}} = \sqrt{(x_{\mathrm{R}} - x_{\mathrm{C}})^2 + (y_{\mathrm{R}} - y_{\mathrm{C}})^2} = \frac{|V|}{|\omega_*|} = \frac{l}{|\tan \gamma_*|}, \tag{23}$$

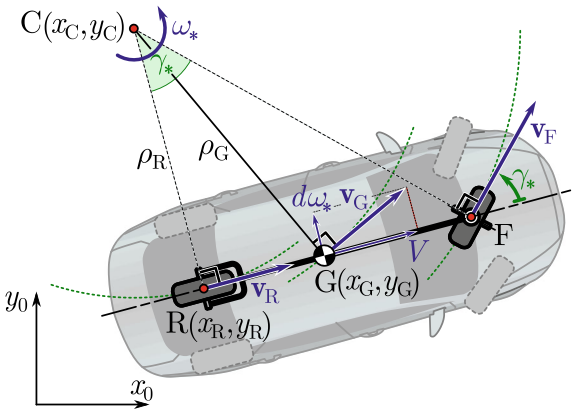

Fig. 4 Steady state cornering for a kinematic bicycle model with the instantaneous center of rotation C and the radii of curvature of points G and R indicated

respectively, where we used that $l > 0$. Note that $d\omega_* = \frac{dV}{l} \tan \gamma_*$ is indeed the lateral velocity component of the center of mass G.

The numerical simulation in Fig. 5 shows the bicycle model in steady state cornering using a constant steering angle of $\gamma(t) \equiv 5°$ at $V = 15\,\text{m/s}$. Other vehicle parameters are listed in Table 1. The circular trajectory of point G in panel (a) corresponds to the initial conditions $x_G(0) = 0\,\text{m}$, $y_G(0) = 0\,\text{m}$ and $\psi(0) = 0°$, and the radius of curvature can be verified using (22). Panels (b)–(d) show the corresponding steady state values of the steering angle [panel (b)], the lateral acceleration of point G [panel (c)] and the lateral constraining forces at the front and rear wheels [panel (d)]. These forces are required to ensure the no side-slip condition of the rigid wheel model (see (16)) and will be compared with the forces calculated based on an elastic tire model in Sect. 4.

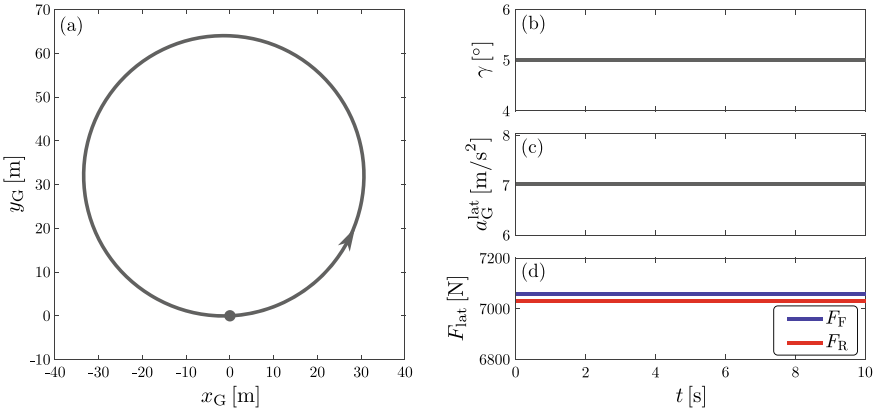

Fig. 5 Numerical simulation of steady state cornering of the kinematic bicycle model (10) at $V = 15\,\text{m/s}$ with steering angle $\gamma = 5°$. **a** Trajectory of the center of mass G; **b** steering angle; **c** lateral acceleration of point G; **d** lateral constraining forces at the front and rear wheels

Table 1 List of vehicle and tire parameters

	Parameter	Value	Unit
l	Vehicle wheelbase	2.8	m
d	Distance between rear axle and center of mass	1.4	m
m	Vehicle mass	2000	kg
J_G	Vehicle mass moment of inertia about the z_0 axis	4000	kgm^2
J_F	Steering system mass moment of inertia about the z_0 axis	2.5	kgm^2
k_t	Steering system torsional stiffness	1000	Nm
k	Tire lateral stiffness per unit length	$1.4 \cdot 10^7$	N/m^2
a	Tire contact patch half-length	0.05	m
μ_0	Static friction coefficient	0.9	
μ	Sliding friction coefficient	0.6	

2.1.2 Transient Dynamics

In Fig. 6, a lane-change maneuver is shown using the proportional steering controller

$$\gamma = -k_y y_R - k_\psi \psi, \tag{24}$$

where k_y and k_ψ are the control gains corresponding to the lateral position of point R and the yaw angle relative to the reference path, respectively. The reference path is assumed to be a straight line along the x_0 axis, and we use the position of the rear axle center point since it is easier to measure. Note that in case of small errors, most steering controllers can typically be reduced to the above form Vörös et al. (2023a), i.e., generating the steering angle based on some combination of the position and angle errors.

Using the selected control gains ($k_y = 0.01\ m^{-1}$ and $k_\psi = 0.8$), the 3.5 m wide lane change maneuver is executed in a smooth manner, without oscillations or overshoot (see Fig. 6a). Panel (b) shows that the maximum steering angle is approximately 2°, which keeps the lateral acceleration low [panel (c)], ensuring a comfortable ride. In panel (d), the lateral constraining forces at the front and rear wheels are plotted.

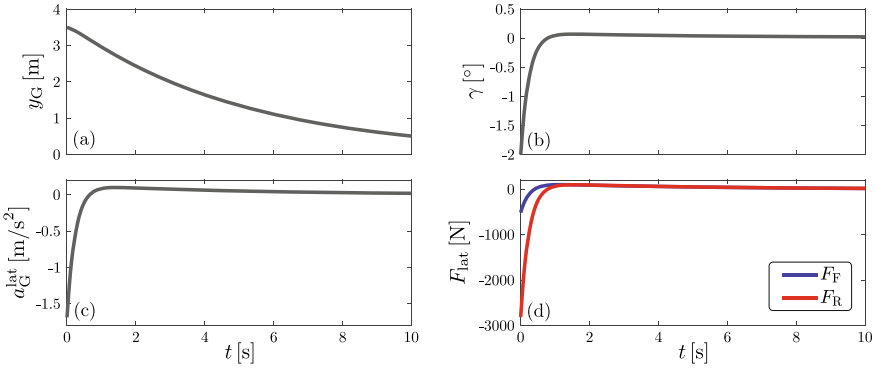

Fig. 6 Numerical simulation of a lane-change maneuver of the kinematic bicycle model (10) at $V = 15$ m/s while utilizing the control law (24) with gains $k_y = 0.01\ \mathrm{m}^{-1}$ and $k_\psi = 0.8$. **a** Lateral position of the center of mass G; **b** steering angle; **c** lateral acceleration of point G; **d** lateral constraining forces at the front and rear wheels

2.2 Kinematic Bicycle Model with Steering Dynamics

In order to highlight the power of the Appellian approach, we consider the model where the longitudinal speed is still restricted but the front wheel is steered by the internal torque T_s, as illustrated in Fig. 7. Now the steering angle γ becomes a configuration coordinate. Thus, we have four generalized coordinates, i.e., the position (x_G, y_G), the yaw angle ψ, and the steering angle γ. The two kinematic constraints in (7) are used to guarantee that there is no sideslip at the skates, and the kinematic constraint (9) maintains the constant longitudinal speed V. Thus, $4 - 3 = 1$ pseudo velocity is needed, and we choose the steering rate

$$\Omega := \dot{\gamma}. \tag{25}$$

The system has $4 - 3\frac{1}{2} = 2.5$ degrees of freedom.

Solving (7), (9), (25), one can obtain

$$\begin{aligned} \dot{x}_G &= V\left(\cos\psi - \frac{d}{l}\sin\psi\tan\gamma\right), \\ \dot{y}_G &= V\left(\sin\psi + \frac{d}{l}\cos\psi\tan\gamma\right), \\ \dot{\psi} &= \frac{V}{l}\tan\gamma, \\ \dot{\gamma} &= \Omega. \end{aligned} \tag{26}$$

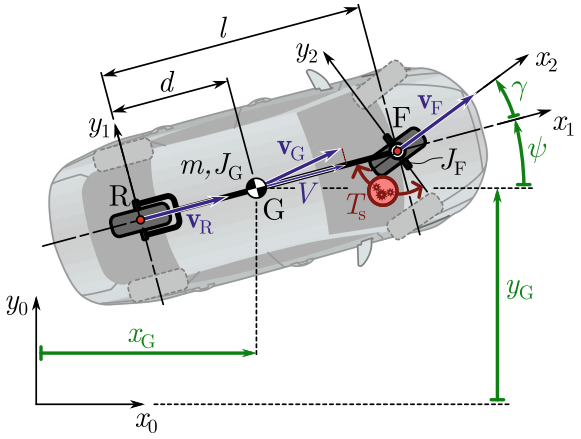

Fig. 7 Single track model (also called bicycle model) of an automobile with rigid wheels and steering dynamics. The geometry, coordinate frames and kinematics are indicated

Taking the time derivative yields

$$\begin{aligned}
\ddot{x}_{\mathrm{G}} &= -\frac{V^2}{l}\tan\gamma\left(\sin\psi + \frac{d}{l}\cos\psi\tan\gamma\right) - \frac{dV}{l}\frac{\sin\psi}{\cos^2\gamma}\Omega,\\
\ddot{y}_{\mathrm{G}} &= \frac{V^2}{l}\tan\gamma\left(\cos\psi - \frac{d}{l}\sin\psi\tan\gamma\right) + \frac{dV}{l}\frac{\cos\psi}{\cos^2\gamma}\Omega,\\
\ddot{\psi} &= \frac{V}{l\cos^2\gamma}\Omega,\\
\ddot{\gamma} &= \dot{\Omega}\,.
\end{aligned} \tag{27}$$

Then considering the mass of the vehicle m, its mass moment of inertia J_{G} about the center of mass G and the mass moment of inertia of the front wheel J_{F} about point F, the acceleration energy of the system becomes

$$\begin{aligned}
S &= \frac{1}{2}m\left(\ddot{x}_{\mathrm{G}}^2 + \ddot{y}_{\mathrm{G}}^2\right) + \frac{1}{2}J_{\mathrm{G}}\ddot{\psi}^2 + \frac{1}{2}J_{\mathrm{F}}\left(\ddot{\psi} + \ddot{\gamma}\right)^2 + \ldots\\
&= \frac{1}{2}J_{\mathrm{F}}\,\dot{\Omega}^2 + \frac{J_{\mathrm{F}}\,V}{l\cos^2\gamma}\Omega\dot{\Omega} + \ldots,
\end{aligned} \tag{28}$$

where the terms that do not contain $\dot{\Omega}$ are incorporated in ....

The virtual power consists of the powers of the steering torque acting on the vehicle body and the front wheel, that is,

$$\delta P = T_{\mathrm{s}}\left(\delta\dot{\psi} + \delta\dot{\gamma}\right) - T_{\mathrm{s}}\,\delta\dot{\psi} = T_{\mathrm{s}}\,\delta\dot{\gamma} = T_{\mathrm{s}}\,\delta\Omega, \tag{29}$$

implying that the pseudo-force is

$$\Pi_{\Omega} = T_{\mathrm{s}}. \tag{30}$$

The Appell equation

$$\frac{\partial S}{\partial \dot{\Omega}} = \Pi_{\Omega}, \tag{31}$$

leads to

$$J_{\mathrm{F}}\,\dot{\Omega} + \frac{J_{\mathrm{F}}\,V}{l\cos^2\gamma}\Omega = T_{\mathrm{s}}. \tag{32}$$

According to (26) and (32) the equations of motion are

$$\begin{aligned}
\dot{x}_{\mathrm{G}} &= V\left(\cos\psi - \frac{d}{l}\sin\psi\tan\gamma\right),\\
\dot{y}_{\mathrm{G}} &= V\left(\sin\psi + \frac{d}{l}\cos\psi\tan\gamma\right),\\
\dot{\psi} &= \frac{V}{l}\tan\gamma,\\
\dot{\gamma} &= \Omega,\\
\dot{\Omega} &= \frac{T_{\mathrm{s}}}{J_{\mathrm{F}}} - \frac{V}{l\cos^2\gamma}\Omega,
\end{aligned} \tag{33}$$

cf. (10). Observe that the last equation contains the steering torque T_{s} as well as a self alignment term that acts as a nonlinear damper in the steering dynamics.

Again, using the position of the rear axle center point R instead of the center of mass G we obtain

$$\begin{aligned}
\dot{x}_{\mathrm{R}} &= V\cos\psi,\\
\dot{y}_{\mathrm{R}} &= V\sin\psi,\\
\dot{\psi} &= \frac{V}{l}\tan\gamma,\\
\dot{\gamma} &= \Omega,\\
\dot{\Omega} &= \frac{T_{\mathrm{s}}}{J_{\mathrm{F}}} - \frac{V}{l\cos^2\gamma}\Omega,
\end{aligned} \tag{34}$$

cf. (13). More models with skates and rigid wheels are discussed in Qin et al. (2022).

Let us consider that the steering torque can be calculated as

$$T_{\mathrm{s}} = k_{\mathrm{t}}\left(\gamma_{\mathrm{d}} - \gamma\right), \tag{35}$$

where γ_{d} is the desired steering angle set by the driver or the automation, while k_{t} represents the torsional stiffness of the steering system or the proportional gain of the steer-by-wire system. Here the control law assigns the desired steering angle

$$\gamma_{\mathrm{d}} = -k_y y_{\mathrm{R}} - k_{\psi}\psi, \tag{36}$$

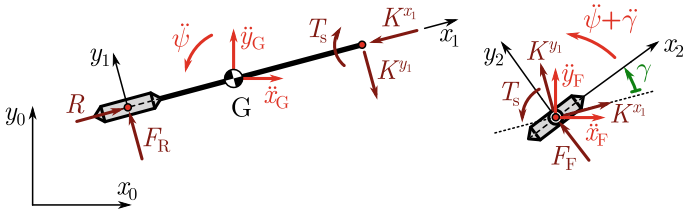

Fig. 8 Free body diagrams of the vehicle body and the front skate when the longitudinal speed is prescribed while the steering is actuated by the internal torque T_s. The constraining forces are also shown

rather than the steering angle itself, cf. (24). Indeed, more complicated steering controllers may be considered as shown, for example, in Beregi et al. (2023).

Again, to obtain the constraining forces, we revert ourselves to the Newtonian approach. We separate the two rigid bodies that constitute the system, namely, the vehicle body and the skate at the front. The corresponding free body diagrams are illustrated in Fig. 8. The components of the internal forces between the skate and the vehicle body are denoted by K^{x_1} and K^{y_1} while the applied steering torque is denoted by T_s. For the sake of simplicity, the same notations are used for the counter forces, but their directions are opposite in the figures according to Newton's third law. Thus, one can apply Newton's second law for the vehicle body and for the front skate, resulting in the equations in the $\mathcal{F}_1$ frame:

$$\begin{aligned}
&m(\ddot{x}_G \cos\psi + \ddot{y}_G \sin\psi) = R - K^{x_1},\\
&\underbrace{m_F}_{\approx 0}(\ddot{x}_F \cos\psi + \ddot{y}_F \sin\psi) = K^{x_1} - F_F \sin\gamma,\\
&m(-\ddot{x}_G \sin\psi + \ddot{y}_G \cos\psi) = F_R - K^{y_1},\\
&\underbrace{m_F}_{\approx 0}(-\ddot{x}_F \sin\psi + \ddot{y}_F \cos\psi) = K^{y_1} + F_F \cos\gamma,\\
&J_G\ddot{\psi} = -d\,F_R - (l-d)K^{y_1} - T_s,\\
&J_F(\ddot{\psi} + \ddot{\gamma}) = T_s\,.
\end{aligned} \tag{37}$$

Considering $m_F = 0$ in the second and the fourth equations yield $K^{x_1} = F_F \sin\gamma$ and $K^{y_1} = -F_F \cos\gamma$ which results in

$$\begin{aligned}
&m(\ddot{x}_G \cos\psi + \ddot{y}_G \sin\psi) = R - F_F \sin\gamma,\\
&m(-\ddot{x}_G \sin\psi + \ddot{y}_G \cos\psi) = F_R + F_F \cos\gamma,\\
&J_G\ddot{\psi} = -d\,F_R + (l-d)F_F \cos\gamma - T_s,\\
&J_F(\ddot{\psi} + \ddot{\gamma}) = T_s,
\end{aligned} \tag{38}$$

where the first two equations are equivalent to those in (14). Substituting (27) into the first three equations one may obtain the constraining forces

$$
\begin{aligned}
F_{\mathrm{R}} &= \frac{V}{l^2}\left(m(l-d)V\tan\gamma - \left(J_{\mathrm{G}} + md^2 - mld\right)\frac{\dot{\gamma}}{\cos^2\gamma}\right) - \frac{T_{\mathrm{s}}}{l}, \\
F_{\mathrm{F}} &= \frac{V}{l^2\cos^3\gamma}\left(mdV\sin\gamma\cos\gamma + \left(J_{\mathrm{G}} + md^2\right)\dot{\gamma}\right) + \frac{T_{\mathrm{s}}}{l\cos\gamma}, \\
R &= \frac{V\sin\gamma}{l^2\cos^3\gamma}\left(J_{\mathrm{G}} + md^2\right)\dot{\gamma} + \frac{T_{\mathrm{s}}}{l}\tan\gamma.
\end{aligned}
\tag{39}
$$

Finally, we remark that using the kinematic constraint (17) instead of (9) and using the kinematic constraint (18) instead of (12), one may derive the handling models for FWD vehicles, i.e., for the case when the speed of the front axle center point F is restricted, while still incorporating the steering dynamics. These calculations are omitted here for the sake of brevity.

2.2.1 Steady State Cornering

The steady state cornering solution of the models (33) and (34) with steering dynamics are still given by (20) and (21), respectively, when considering a constant desired steering angle $\gamma_{\mathrm{d}}(t) \equiv \gamma_{\mathrm{d}}^{*} = \gamma_{*}$. Correspondingly, the radii of curvature are still given by (22) and (23).

Since extending the bicycle model with rigid wheels with the consideration of tire dynamics does not affect the steady state solution, numerical simulation of steady state cornering leads to the same results as in Fig. 5.

2.2.2 Transient Dynamics

As shown in in Fig. 9, the lane change maneuver with steering dynamics (35) and control law (24) also shows similar characteristics in terms of the lateral position of the vehicle (cf. panel (a) with Fig. 6a). However, the mismatch between the desired and the realized steering angles causes strong transient oscillations in γ [panel (b)] which also show up in the lateral acceleration [panel (c)] and the tire forces [panel (d)]. Therefore, even though the vehicle trajectory is largely unaffected by these oscillations of the steering system, a bad design may cause significant problems both in terms of passenger comfort and tire wear. In order to avoid these effects, the torsional stiffness (or corresponding lower-level control parameter) k_{t} should be tuned carefully.

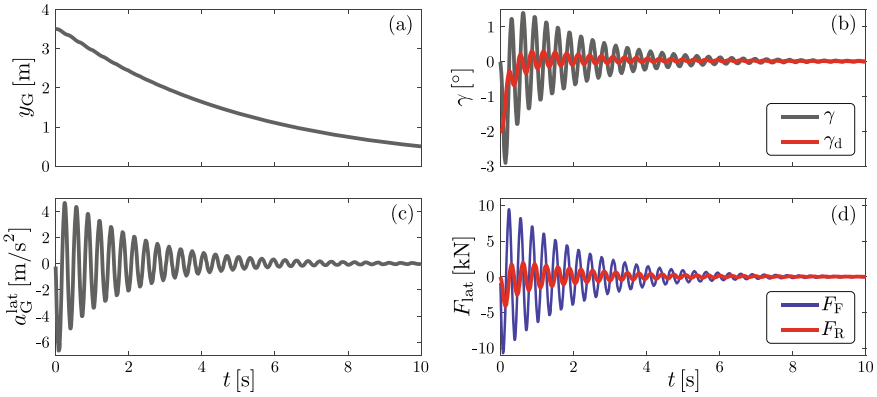

Fig. 9 Numerical simulation of a lane-change maneuver of the kinematic bicycle model with steering dynamics given in (33) and (35) at $V = 15$ m/s while utilizing the control law (36) with gains $k_y = 0.01\,\mathrm{m}^{-1}$ and $k_\psi = 0.8$. **a** Lateral position of the center of mass G; **b** desired (red) and realized (black) steering angle; **c** lateral acceleration of point G; **d** lateral constraining forces at the front and rear wheels

3 Lateral Brush Tire Model

In this section, we build a tire model from first principles, which will be used to improve the fidelity of the vehicle handling model in the next section.

Figure 10 compares the rigid wheel model used in the previous section [see panel (a)] to the so-called brush tire model described in detail below [see panel (b)]. Observe that for the rigid wheel the velocity vector $\mathbf{v}_C$ of the wheel center point C is aligned with the wheel plane while in case of the tire it forms a slip angle α with the wheel plane. In the meantime the wheel rotates with the angular velocity ω_y around its axle and swivels about the vertical direction with angular velocity $\omega_z = \dot{\psi}$. All vectors are resolved in the (x, y, z) frame which travels with the wheel with its origin attached to the wheel center C.

It is assumed that the tire consists of an unstretchable band with (infinitesimally small) brush-like elements attached to it. These brushes can deform in the lateral direction along the tire-ground contact. The length of the contact patch is $2a$ and the effective wheel radius is $r = \sqrt{R^2 - a^2}$, see Fig. 10c.

3.1 Tire Deformation Along the Contact Patch

Let us focus on a single bristle QP. Point Q is attached to the unstretchable band while point P touches the road surface and it either sticks to the ground (in which case it has zero velocity) or it slides on the ground. The lateral deformation of the bristle (i.e., the distance between Q and P in the y direction) is denoted by $\eta(x, t)$

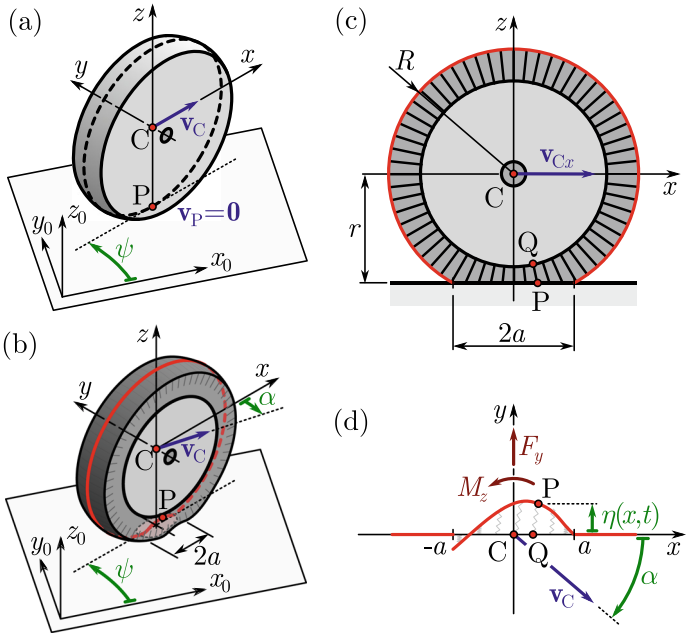

Fig. 10 Panels **a** and **b** compare a model of a rigid wheel and a model of a wheel with elastic tire. The red curve indicates the center line of the tire which deforms along the contact patch of length $2a$. As a consequence, the velocity of the wheel center C does not align with the wheel plane but forms a slip angle α. Panel **c** shows the side view of the wheel highlighting the geometry of the tire as well as the thread element QP. Panel **d** depicts the lateral tire deformation $\eta(x, t)$ through the top view image

which depends on the longitudinal position x along the contact patch and time t, see Fig. 10d. The resultant lateral force F_y acts at the center of the contact patch, while the asymmetry of force distribution is captured by the aligning moment M_z.

The position vector of point P can given as

$$\mathbf{r}_{\mathrm{CP}} = \begin{bmatrix} x \\ \eta(x,t) \\ -r \end{bmatrix}. \tag{40}$$

Let us define the point P′ as a point fixed to the reference frame that coincides with P at a certain time instant. The velocity of P′ with respect to the road surface is $\mathbf{v}_{\mathrm{P,carr}}$ and the relative velocity of P with respect to the reference frame is $\mathbf{v}_{\mathrm{P,rel}}$. These can be written as:

$$\begin{aligned}\mathbf{v}_{\mathrm{P,carr}} &= \mathbf{v}_{\mathrm{C}} + \boldsymbol{\omega} \times \mathbf{r}_{\mathrm{CP}} \\ &= \begin{bmatrix} v\cos\alpha \\ -v\sin\alpha \\ 0 \end{bmatrix} + \begin{bmatrix} 0 \\ 0 \\ \dot{\psi} \end{bmatrix} \times \begin{bmatrix} x \\ \eta(x,t) \\ -r \end{bmatrix} = \begin{bmatrix} v\cos\alpha - \dot{\psi}\eta(x,t) \\ -v\sin\alpha + \dot{\psi}x \\ 0 \end{bmatrix}, \\ \mathbf{v}_{\mathrm{P,rel}} &= \mathring{\mathbf{r}}_{\mathrm{CP}} \\ &= \begin{bmatrix} \dot{x} \\ \frac{\mathrm{d}}{\mathrm{d}t}\eta(x,t) \\ 0 \end{bmatrix} = \begin{bmatrix} \dot{x} \\ \dot{\eta}(x,t) + \dot{x}\,\eta'(x,t) \\ 0 \end{bmatrix},\end{aligned} \tag{41}$$

where $\boldsymbol{\omega}$ is the angular velocity of the moving frame (x, y, z), the circle represents the derivative in this moving frame, $v := |\mathbf{v}_{\mathrm{C}}| > 0$ denotes the speed of the wheel center C, while $\dot{\eta}(x,t)$ and $\eta'(x,t)$ denote partial derivatives with respect to time t and space x, respectively. Then the velocity of point P can be obtained as

$$\mathbf{v}_{\mathrm{P}} = \mathbf{v}_{\mathrm{P,carr}} + \mathbf{v}_{\mathrm{P,rel}} = \begin{bmatrix} v\cos\alpha - \dot{\psi}\eta(x,t) + \dot{x} \\ -v\sin\alpha + \dot{\psi}x + \dot{\eta}(x,t) + \dot{x}\,\eta'(x,t) \\ 0 \end{bmatrix}. \tag{42}$$

When the friction force is large enough, it can ensure that point P sticks to the ground, that is,

$$\mathbf{v}_{\mathrm{P}} = \mathbf{0}\,. \tag{43}$$

Substituting (42) and eliminating $\dot{x}$ leads to the partial differential equation (PDE):

$$\dot{\eta}(x,t) = v\sin\alpha - x\dot{\psi} + \eta'(x,t)\left(v\cos\alpha - \eta(x,t)\dot{\psi}\right). \tag{44}$$

In addition, the assumption that no deformation occurs at the leading edge leads to the boundary condition

$$\eta(a,t) = 0. \tag{45}$$

The PDE (44) is nonlinear in $\eta(x,t)$ and (44), (45) can be solved (numerically) once the velocity of the wheel center (given by the speed v and the slip angle α) and the angular velocity component $\dot{\psi}$ are given. Indeed, these may be functions of time.

Now, consider the case when v, α and ψ are constants (i.e., $\dot{\psi} \equiv 0$). Then, (44) simplifies to

$$\dot{\eta}(x,t) = v\sin\alpha + \eta'(x,t)v\cos\alpha, \tag{46}$$

which is a linear PDE. The analytical solution of (45), (46) can be obtained by the method of characteristics. Here we focus on the steady state solution $\eta(x,t) = \eta_*(x)$. In this case the PDE (46) reduces to the ODE

$$\eta_*'(x) = -\tan\alpha, \tag{47}$$

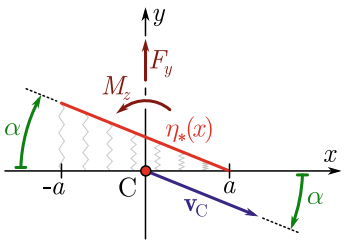

Fig. 11 Steady state lateral deformation (48) when all brush elements sticks to the road

and using the boundary condition $\eta_*(a) = 0$ we obtain the solution

$$\eta_*(x) = (a - x)\tan\alpha. \tag{48}$$

Figure 11 shows that the deformation of the tread elements along the contact patch aligns with the velocity vector v_C of the wheel center C in steady state. Assuming that v, α and ψ change slower than the deformation dynamics in the contact patch, the form

$$\eta(x,t) = (a - x)\tan\alpha(t), \tag{49}$$

is often used in the literature.

3.2 Lateral Force and Aligining Moment

As a next step, let us calculate the lateral force F_y and the aligning moment M_z based on the shear deformation of the tread elements. As illustrated in Fig. 12, the angle of deformation of a single element is

$$\gamma(x,t) = \arctan\frac{\eta(x,t)}{h} \approx \frac{\eta(x,t)}{h}, \tag{50}$$

where h is the tire thickness. The corresponding lateral force is

$$Gw\,\gamma(x,t) \approx \frac{Gw}{h}\eta(x,t), \tag{51}$$

where G is the shear modulus and w is the tire width. Let us define the lateral stiffness per unit length as

$$k = \frac{Gw}{h}. \tag{52}$$

Then, the lateral force and the aligning moment can be calculated as

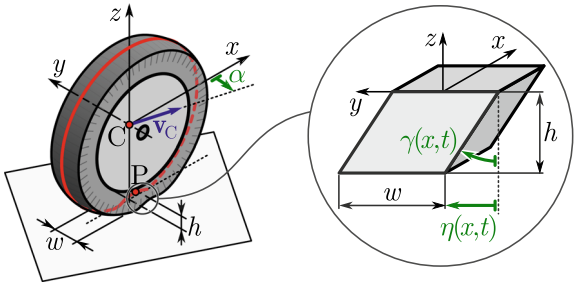

Fig. 12 Shear deformation of a tread element

$$F_y(t) = \int_{-a}^{a} k\,\eta(x,t)\,\mathrm{d}x, \qquad M_z(t) = \int_{-a}^{a} x\,k\,\eta(x,t)\,\mathrm{d}x. \tag{53}$$

Assuming that the tire elements stick to the ground all along the contact patch, the steady state solution (48) holds for $x \in [-a, a]$. This yields the steady state lateral force

$$F_y^* = \int_{-a}^{a} k\,\eta_*(x)\,\mathrm{d}x = \int_{-a}^{a} k\,(a-x)\tan\alpha\,\mathrm{d}x = 2ka^2\tan\alpha = C\tan\alpha, \tag{54}$$

where we introduced the cornering stiffness $C = 2ka^2$. A more general definition of the cornering stiffness is based on the slope of the lateral force characteristic at zero slip angle:

$$C = \left.\frac{\mathrm{d}F_y^*}{\mathrm{d}\alpha}\right|_{\alpha=0}. \tag{55}$$

The steady state aligning moment can similarly be determined by integration along the contact patch:

$$M_z^* = \int_{-a}^{a} x\,k\,\eta_*(x)\,\mathrm{d}x = \int_{-a}^{a} x\,k\,(a-x)\tan\alpha\,\mathrm{d}x = -C\frac{a}{3}\tan\alpha. \tag{56}$$

3.2.1 Sliding at the Rear of the Contact Patch

Whether a tire element sticks to the ground depends on the available friction, which is determined by the friction coefficient and vertical force at that location. Namely the condition for sticking to the ground is

$$k\,\eta(x,t) \le \mu_0\,w\,p(x), \tag{57}$$

where μ_0 is the static friction coefficient, w is the width of the tire, and $p(x)$ is the pressure at location x. Once a tire particle slides we have

$$k\,\eta(x,t) = \mu\, w\, p(x), \tag{58}$$

where μ is the sliding friction coefficient. This may be used to obtain the deformation $\eta(x,t)$ instead of using the PDE (44) or the PDE (46). Indeed, when sliding occurs at some part of the contact patch, it influences the lateral force and the aligning moment defined in (53) as explained below.

In this book chapter, we assume the parabolic pressure distribution

$$p(x) = p_{\max}\left(1 - \left(\frac{x}{a}\right)^2\right), \tag{59}$$

which is depicted in Fig. 13a. The corresponding vertical load is

$$F_z = \int_{-a}^{a} p_{\max}\left(1 - \left(\frac{x}{a}\right)^2\right) w\,\mathrm{d}x = p_{\max}\frac{4a}{3}w. \tag{60}$$

From this, we can calculate

$$p_{\max} = \frac{3F_z}{4aw}, \tag{61}$$

leading to the pressure distribution

$$p(x) = \frac{3F_z}{4aw}\left(1 - \left(\frac{x}{a}\right)^2\right). \tag{62}$$

Figure 13b shows the limits corresponding to (57) and (58) as green and blue parabolas, respectively. The steady state solution (48) is also shown as the red line with gradient $\tan\alpha$. That is, at the front of the contact patch we have

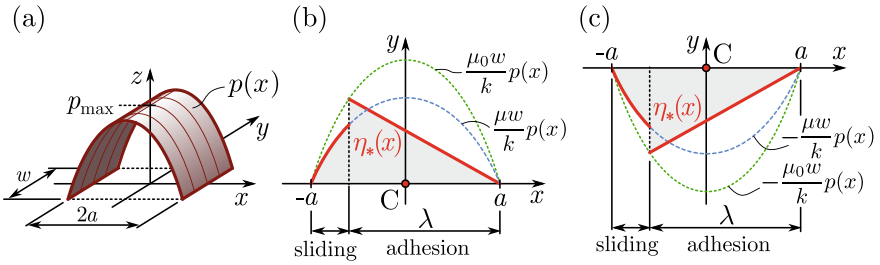

Fig. 13 **a** Parabolic pressure distribution (59). **b** Steady state lateral deformation (65) for positive slip angle. **c** Steady state lateral deformation (78) for negative slip angle

$$\eta_*(x) = (a-x)\tan\alpha \le \frac{\mu_0 w}{k} p(x) = \frac{3\mu_0 F_z}{4ka}\left(1-\left(\frac{x}{a}\right)^2\right), \tag{63}$$

and this is referred to as the adhesion region. At the rear of the contact patch sliding occurs, which yields

$$\eta_*(x) = \frac{\mu w}{k} p(x) = \frac{3\mu F_z}{4ka}\left(1-\left(\frac{x}{a}\right)^2\right). \tag{64}$$

These can be summarized as

$$\eta_*(x) = \begin{cases} (a-x)\tan\alpha & \text{if} \quad x \in [a-\lambda, a], \\ \frac{3\mu F_z}{4ka}\left(1-\left(\frac{x}{a}\right)^2\right) & \text{if} \quad x \in [-a, a-\lambda), \end{cases} \tag{65}$$

where λ denotes the adhesion length. At $x = a-\lambda$ equality happens in (63) and this results in

$$\lambda \tan\alpha = \frac{3\mu_0 F_z}{4ka}\frac{a^2-(a-\lambda)^2}{a^2}, \tag{66}$$

which can be solved for the adhesion length

$$\lambda = 2a - \frac{4ka^3}{3\mu_0 F_z}\tan\alpha. \tag{67}$$

3.2.2 Steady State Lateral Force

Using the steady state deformation (65) in (53), one may calculate the lateral force

$$\begin{aligned} F_y^* &= \int_{-a}^{a} k\,\eta_*(x)\,\mathrm{d}x = \int_{a-\lambda}^{a} k(a-x)\tan\alpha\,\mathrm{d}x + \int_{-a}^{a-\lambda} \frac{3\mu F_z}{4a}\left(1-\left(\frac{x}{a}\right)^2\right)\mathrm{d}x \\ &= \frac{k}{2}\lambda^2\tan\alpha + \frac{\mu F_z}{4a^3}(2a-\lambda)^2(a+\lambda). \end{aligned} \tag{68}$$

Substituting (67) results in

$$F_y^* = 2ka^2\tan\alpha - \frac{\left(2ka^2\right)^2}{3\mu_0 F_z}\left(2-\frac{\mu}{\mu_0}\right)\tan^2\alpha + \frac{\left(2ka^2\right)^3}{(3\mu_0 F_z)^2}\left(1-\frac{2\mu}{3\mu_0}\right)\tan^3\alpha. \tag{69}$$

Note that the cornering stiffness can be calculated using (55), that yields

$$C = \left.\frac{\mathrm{d}F_y^*}{\mathrm{d}\alpha}\right|_{\alpha=0} = 2ka^2, \tag{70}$$

which is indeed the coefficient of the linear term in (69).

One may observe in Fig. 13b that as the gradient $\tan\alpha$ increases, the adhesion region decreases, and at some critical value α_{cr} of the slip angle the adhesion length λ becomes zero. Then, the adhesion region disappears and sliding occurs along the entire contact patch. Substituting $\lambda = 0$ into (67), the critical slip angle becomes

$$\alpha_{\mathrm{cr}} = \arctan\frac{3\mu_0 F_z}{2ka^2}. \tag{71}$$

That is, (68) only holds for $0 \le \alpha \le \alpha_{\mathrm{cr}}$. For $\alpha > \alpha_{\mathrm{cr}}$ the deformation is given by (64) for $x \in [-a, a]$ and the steady state lateral force becomes

$$F_y^* = \int_{-a}^{a} k\,\eta_*(x)\,\mathrm{d}x = \int_{-a}^{a} \frac{3\mu F_z}{4a}\left(1 - \left(\frac{x}{a}\right)^2\right)\mathrm{d}x = \mu F_z, \tag{72}$$

which confirms that sliding happens on the whole contact patch. Using (69), it can be shown that

$$\left.F_y^*\right|_{\alpha=\alpha_{\mathrm{cr}}} = \mu F_z, \qquad \left.\frac{\mathrm{d}F_y^*}{\mathrm{d}\alpha}\right|_{\alpha=\alpha_{\mathrm{cr}}} = 0, \tag{73}$$

that is, the curve of the force characteristic is continuous and smooth at $\alpha = \alpha_{\mathrm{cr}}$; see Fig. 14a.

For negative slip angles $\alpha < 0$, the condition for sticking to the ground becomes

$$k\,\eta(x,t) \ge -\mu_0\, w\, p(x), \tag{74}$$

while for sliding we have

$$k\,\eta(x,t) = -\mu\, w\, p(x), \tag{75}$$

cf. (57) and (58). Consequently, in steady state the lateral deformation in the adhesion region is

$$\eta_*(x) = (a - x)\tan\alpha \ge -\frac{\mu_0 w}{k}p(x) = -\frac{3\mu_0 F_z}{4ka}\left(1 - \left(\frac{x}{a}\right)^2\right), \tag{76}$$

while in the sliding region it is

$$\eta_*(x) = -\frac{\mu w}{k}p(x) = -\frac{3\mu F_z}{4ka}\left(1 - \left(\frac{x}{a}\right)^2\right). \tag{77}$$

These can be summarized as

$$\eta_*(x) = \begin{cases} (a-x)\tan\alpha & \text{if} \quad x \in [a-\lambda, a], \\ -\frac{3\mu F_z}{4ka}\left(1-\left(\frac{x}{a}\right)^2\right) & \text{if} \quad x \in [-a, a-\lambda), \end{cases} \tag{78}$$

cf. (63), (64), and (65). Considering equality in (76) when $x = a - \lambda$, we obtain the adhesion length

$$\lambda = 2a + \frac{4ka^3}{3\mu_0 F_z}\tan\alpha, \tag{79}$$

cf. (67).

Then using the steady state deformation (78) in (53), one may calculate the lateral force

$$\begin{aligned} F_y^* &= \int_{-a}^{a} k\,\eta_*(x)\,\mathrm{d}x = \int_{a-\lambda}^{a} k(a-x)\tan\alpha\,\mathrm{d}x - \int_{-a}^{a-\lambda} \frac{3\mu F_z}{4a}\left(1-\left(\frac{x}{a}\right)^2\right)\mathrm{d}x \\ &= \frac{k}{2}\lambda^2\tan\alpha - \frac{\mu F_z}{4a^3}(2a-\lambda)^2(a+\lambda), \end{aligned} \tag{80}$$

cf. (68). Substituting (79) yields

$$F_y^* = 2ka^2\tan\alpha + \frac{\left(2ka^2\right)^2}{3\mu_0 F_z}\left(2-\frac{\mu}{\mu_0}\right)\tan^2\alpha + \frac{\left(2ka^2\right)^3}{\left(3\mu_0 F_z\right)^2}\left(1-\frac{2\mu}{3\mu_0}\right)\tan^3\alpha, \tag{81}$$

where only the sign of the second term is changed compared to (69). Again (81) only holds for $\bar{\alpha}_{\mathrm{cr}} \le \alpha \le 0$. For $\alpha < \bar{\alpha}_{\mathrm{cr}}$ the deformations is given by (77) for $x \in [-a, a]$ and we have

$$F_y^* = \int_{-a}^{a} k\,\eta_*(x)\,\mathrm{d}x = -\int_{-a}^{a} \frac{3\mu F_z}{4a}\left(1-\left(\frac{x}{a}\right)^2\right)\mathrm{d}x = -\mu F_z, \tag{82}$$

cf. (72). Substituting $\lambda = 0$ into (79) results in

$$\bar{\alpha}_{\mathrm{cr}} = -\arctan\frac{3\mu_0 F_z}{2ka^2} = -\alpha_{\mathrm{cr}}, \tag{83}$$

cf. (71). Using (81), one may also show that the force characteristic is continuous and smooth at $\alpha = -\alpha_{\mathrm{cr}}$, that is,

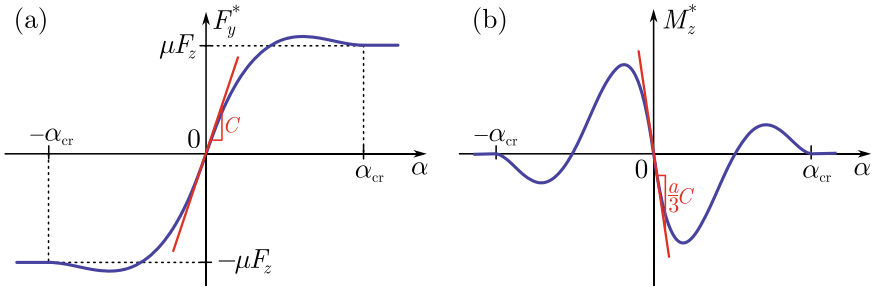

Fig. 14 **a** Steady state lateral force characteristic (85) and (86). **b** Steady state aligning moment characteristic (93) and (94)

$$F_y^*\Big|_{\alpha=-\alpha_{cr}} = -\mu F_z, \qquad \frac{\mathrm{d}F_y^*}{\mathrm{d}\alpha}\Big|_{\alpha=-\alpha_{cr}} = 0, \tag{84}$$

cf. (73) and see Fig. 14a.

In summary, formulae (69), (72), (81), (82) can be written as

$$F_y^* = \begin{cases} \Phi_1 \tan\alpha + \Phi_2 \tan^2\alpha \,\mathrm{sgn}(\alpha) + \Phi_3 \tan^3\alpha & \text{if} \quad 0 \le |\alpha| \le \alpha_{cr}, \\ \mu F_z \,\mathrm{sgn}(\alpha) & \text{if} \quad |\alpha| > \alpha_{cr}, \end{cases} \tag{85}$$

where

$$\Phi_1 = C, \quad \Phi_2 = -\frac{C^2}{3\mu_0 F_z}\left(2 - \frac{\mu}{\mu_0}\right), \quad \Phi_3 = \frac{C^3}{(3\mu_0 F_z)^2}\left(1 - \frac{2\mu}{3\mu_0}\right), \tag{86}$$

the cornering stiffness C is given by (70), and α_{cr} is given by (71). This model is depicted in Fig. 14a. Note that the model with simplification $\mu = \mu_0$ is often referred to as the Fiala model (Fiala, 1954).

3.2.3 Steady State Aligning Moment

Now we utilize (53) to calculate the aligning moment in steady state. For $0 \le \alpha \le \alpha_{cr}$ we utilize (65) which yields

$$
\begin{aligned}
M_z^* &= \int_{-a}^{a} x\, k\, \eta_*(x)\, \mathrm{d}x \\
&= \int_{a-\lambda}^{a} x\, k(a-x)\tan\alpha\, \mathrm{d}x + \int_{-a}^{a-\lambda} x\, \frac{3\mu F_z}{4a}\left(1-\left(\frac{x}{a}\right)^2\right) \mathrm{d}x \\
&= \frac{k}{6}(3a-2\lambda)\lambda^2\tan\alpha - \frac{3\mu F_z}{16a^3}(2a-\lambda)^2\lambda^2.
\end{aligned}
\tag{87}
$$

Substituting the adhesion length (67) results in

$$
\begin{aligned}
M_z^* = &-\frac{a}{3}2ka^2\tan\alpha + a\frac{(2ka^2)^2}{3\mu_0 F_z}\left(2-\frac{\mu}{\mu_0}\right)\tan^2\alpha \\
&- 3a\frac{(2ka^2)^3}{(3\mu_0 F_z)^2}\left(1-\frac{2\mu}{3\mu_0}\right)\tan^3\alpha + a\frac{(2ka^2)^4}{(3\mu_0 F_z)^3}\left(\frac{4}{3}-\frac{\mu}{\mu_0}\right)\tan^4\alpha.
\end{aligned}
\tag{88}
$$

Similarly for $-\alpha_{\mathrm{cr}} \le \alpha \le 0$ we use (78) to obtain

$$
\begin{aligned}
M_z^* &= \int_{-a}^{a} x\, k\, \eta_*(x)\, \mathrm{d}x \\
&= \int_{a-\lambda}^{a} x\, k(a-x)\tan\alpha\, \mathrm{d}x - \int_{-a}^{a-\lambda} x\, \frac{3\mu F_z}{4a}\left(1-\left(\frac{x}{a}\right)^2\right) \mathrm{d}x \\
&= \frac{k}{6}(3a-2\lambda)\lambda^2\tan\alpha + \frac{3\mu F_z}{16a^3}(2a-\lambda)^2\lambda^2,
\end{aligned}
\tag{89}
$$

cf. (87). Substituting the adhesion length (79) yields

$$
\begin{aligned}
M_z^* = &-\frac{a}{3}2ka^2\tan\alpha - a\frac{(2ka^2)^2}{3\mu_0 F_z}\left(2-\frac{\mu}{\mu_0}\right)\tan^2\alpha \\
&- 3a\frac{(2ka^2)^3}{(3\mu_0 F_z)^2}\left(1-\frac{2\mu}{3\mu_0}\right)\tan^3\alpha - a\frac{(2ka^2)^4}{(3\mu_0 F_z)^3}\left(\frac{4}{3}-\frac{\mu}{\mu_0}\right)\tan^4\alpha,
\end{aligned}
\tag{90}
$$

where only the signs of the second and fourth terms are changed compared to (88).

For $\alpha > \alpha_{\mathrm{cr}}$ and $\alpha < -\alpha_{\mathrm{cr}}$ the deformation is given by (64) and (77), respectively, for $x \in [-a, a]$. These result in

$$
M_z^* = \int_{-a}^{a} x\, k\, \eta_*(x)\, \mathrm{d}x = \pm \int_{-a}^{a} x\, \frac{3\mu F_z}{4a}\left(1-\left(\frac{x}{a}\right)^2\right) \mathrm{d}x = 0. \tag{91}
$$

Using (88) and (90) it can be shown that the characteristic is continuous and smooth at $\alpha = \pm\alpha_{\text{cr}}$, that is,

$$M_z^*\Big|_{\alpha=\pm\alpha_{\text{cr}}} = 0, \qquad \frac{\mathrm{d}M_z^*}{\mathrm{d}\alpha}\Big|_{\alpha=\pm\alpha_{\text{cr}}} = 0, \tag{92}$$

see Fig. 14b.

Formulae (88), (90) and (91) can be summarized as

$$M_z^* = \begin{cases} \Psi_1 \tan\alpha + \Psi_2 \tan^2\alpha \,\operatorname{sgn}(\alpha) + \Psi_3 \tan^3\alpha + \Psi_4 \tan^4\alpha \,\operatorname{sgn}(\alpha) \\ \qquad\qquad\qquad\qquad\qquad\qquad\qquad\qquad \text{if} \quad 0 \le |\alpha| \le \alpha_{\text{cr}}, \\ 0 \qquad\qquad\qquad\qquad\qquad\qquad\qquad\qquad\quad \text{if} \quad |\alpha| > \alpha_{\text{cr}}, \end{cases} \tag{93}$$

where

$$\Psi_1 = -\frac{a}{3}\Phi_1, \quad \Psi_2 = -a\Phi_2, \quad \Psi_3 = -3a\Phi_3, \quad \Psi_4 = a\frac{C^4}{(3\mu_0 F_z)^3}\left(\frac{4}{3} - \frac{\mu}{\mu_0}\right), \tag{94}$$

and Φ_1, Φ_2, Φ_3 are given in (86) while α_{cr} is given in (71). The aligning moment is depicted in Fig. 14b.

We remark that the physics-based characteristics (85) and (93) contain a key feature which is not captured by popular data-based models like the magic formula (Mi et al., 2020). Namely, the function $\operatorname{sgn}(\alpha)$ in the second order terms makes these characteristics non-differentiable in the second order at $\alpha = 0$. This type of nonlinearity arises from the sticking/sliding transitions between the tire particles and the ground and it has important implications on the nonlinear behavior of the vehicle (Beregi et al., 2019).

4 Vehicles Models with Elastic Tires

In this section, we extend the single track models established in Sect. 2 with the tire model derived in Sect. 3.

4.1 Bicycle Model with Elastic Tires

The single track vehicle model with tires, also called the dynamic bicycle model, is shown in Fig. 15. As discussed in Sect. 3, the kinematic constraints of the rolling

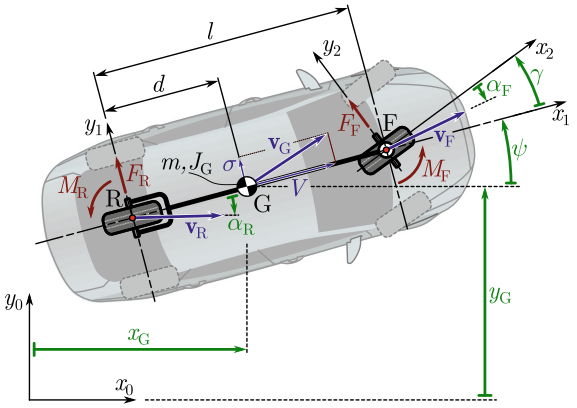

Fig. 15 Single track model of an automobile with elastic tires with geometry, coordinate frames, kinematics, tire forces and moments indicated

wheels are violated due to the side slips of the tires. The corresponding tire deformations generate the lateral forces $\mathbf{F}_R, \mathbf{F}_F$ and aligning moments M_R, M_F at the front and rear tires.

To describe the position and orientation of the vehicle, we still need three configuration coordinates. Here we use the position of the center of gravity G, that is, (x_G, y_G), and the yaw angle ψ. Without constraints, the system would have 3 degrees of freedom. Since we focus on the handling behavior, we eliminate the longitudinal dynamics by restricting the longitudinal velocity. This yields the kinematic constraint

$$\dot{x}_G \cos\psi + \dot{y}_G \sin\psi = V\,, \tag{95}$$

which has already been utilized in the models with rigid wheels, see (9). This means that we need to select $3 - 1 = 2$ pseudo velocities. We choose the lateral velocity of point G, denoted by σ, and the yaw rate ω:

$$\begin{aligned} \sigma &= -\dot{x}_G \sin\psi + \dot{y}_G \cos\psi, \\ \omega &= \dot{\psi}. \end{aligned} \tag{96}$$

The single kinematic constraint (95) results in $3 - \frac{1}{2} = 2.5$ degrees of freedom overall.

The system of Eqs. (95) and (96) can be solved for the generalized velocities:

$$\begin{aligned} \dot{x}_G &= V\cos\psi - \sigma\sin\psi, \\ \dot{y}_G &= V\sin\psi + \sigma\cos\psi, \\ \dot{\psi} &= \omega. \end{aligned} \tag{97}$$

Taking the derivative with respect to time results in

$$\begin{aligned}\ddot{x}_{\mathrm{G}} &= -V\omega\sin\psi - \dot{\sigma}\sin\psi - \sigma\omega\cos\psi,\\ \ddot{y}_{\mathrm{G}} &= V\omega\cos\psi + \dot{\sigma}\cos\psi - \sigma\omega\sin\psi,\\ \ddot{\psi} &= \dot{\omega},\end{aligned} \tag{98}$$

where $\ddot{x}_{\mathrm{G}}$ and $\ddot{y}_{\mathrm{G}}$ are the acceleration components of the center of mass G in the Earth-fixed frame $\mathcal{F}_0$, see (3).

We remark that the velocity vector of point G in the vehicle-fixed frame $\mathcal{F}_1$ is given by

$$\mathbf{v}_{\mathrm{G}} = \begin{bmatrix} \dot{x}_{\mathrm{G}}\cos\psi + \dot{y}_{\mathrm{G}}\sin\psi \\ -\dot{x}_{\mathrm{G}}\sin\psi + \dot{y}_{\mathrm{G}}\cos\psi \end{bmatrix}_{\mathcal{F}_1} = \begin{bmatrix} V \\ \sigma \end{bmatrix}_{\mathcal{F}_1}, \tag{99}$$

cf. (5), (95) and (96). Accordingly, the acceleration in the vehicle-fixed frame $\mathcal{F}_1$ can be calculated as

$$\mathbf{a}_{\mathrm{G}} = \begin{bmatrix} \ddot{x}_{\mathrm{G}}\cos\psi + \ddot{y}_{\mathrm{G}}\sin\psi \\ -\ddot{x}_{\mathrm{G}}\sin\psi + \ddot{y}_{\mathrm{G}}\cos\psi \end{bmatrix}_{\mathcal{F}_1} = \begin{bmatrix} -\sigma\omega \\ V\omega + \dot{\sigma} \end{bmatrix}_{\mathcal{F}_1}, \tag{100}$$

where the corresponding acceleration components are referred to as the longitudinal acceleration and the lateral acceleration.

Then the acceleration energy of the system becomes

$$\begin{aligned} S &= \frac{1}{2}m\left(\ddot{x}_{\mathrm{G}}^2 + \ddot{y}_{\mathrm{G}}^2\right) + \frac{1}{2}J_{\mathrm{G}}\ddot{\psi}^2 + \ldots\\ &= \frac{1}{2}m\left(\dot{\sigma}^2 + 2V\omega\dot{\sigma}\right) + \frac{1}{2}J_{\mathrm{G}}\dot{\omega}^2 + \ldots, \end{aligned} \tag{101}$$

where the terms which do not contain $\dot{\sigma}$ or $\dot{\omega}$ are incorporated in $\ldots$.

The virtual power of the active forces $\mathbf{F}_{\mathrm{R}}, \mathbf{F}_{\mathrm{F}}$ and torques $M_{\mathrm{R}}, M_{\mathrm{F}}$ can be calculated as

$$\begin{aligned} \delta P &= \mathbf{F}_{\mathrm{R}}\cdot\delta\mathbf{v}_{\mathrm{R}} + \mathbf{F}_{\mathrm{F}}\cdot\delta\mathbf{v}_{\mathrm{F}} + M_{\mathrm{R}}\,\delta\dot{\psi} + M_{\mathrm{F}}\,\delta\left(\dot{\psi}+\dot{\gamma}\right)\\ &= \mathbf{F}_{\mathrm{R}}\cdot\delta\mathbf{v}_{\mathrm{R}} + \mathbf{F}_{\mathrm{F}}\cdot\delta\mathbf{v}_{\mathrm{F}} + \left(M_{\mathrm{R}}+M_{\mathrm{F}}\right)\delta\omega, \end{aligned} \tag{102}$$

where we used that $\dot{\psi} = \omega$ (see (97)) and that the virtual steering rate is zero, i.e., $\delta\dot{\gamma} = 0$. The velocity vectors of points R and F are

$$\mathbf{v}_{\mathrm{R}} = \mathbf{v}_{\mathrm{G}} + \boldsymbol{\omega}\times\mathbf{r}_{\mathrm{GR}} = \begin{bmatrix} V \\ \sigma - d\omega \end{bmatrix}_{\mathcal{F}_1}, \tag{103}$$

and

$$\mathbf{v}_{\mathrm{F}} = \mathbf{v}_{\mathrm{G}} + \boldsymbol{\omega}\times\mathbf{r}_{\mathrm{GF}} = \begin{bmatrix} V \\ \sigma + (l-d)\,\omega \end{bmatrix}_{\mathcal{F}_1}, \tag{104}$$

respectively, where $\boldsymbol{\omega} = \begin{bmatrix} 0 & 0 & \omega \end{bmatrix}^{\top}_{\mathcal{F}_1}$ is the angular velocity vector of the vehicle while $\mathbf{r}_{\mathrm{GR}} = \begin{bmatrix} 0 & -d & 0 \end{bmatrix}^{\top}_{\mathcal{F}_1}$ and $\mathbf{r}_{\mathrm{GF}} = \begin{bmatrix} 0 & l-d & 0 \end{bmatrix}^{\top}_{\mathcal{F}_1}$ and we did not spell out the third (zero) components of the vectors in (103) and (104) for simplicity. Note that these results can also be obtained by substituting (97) into (5). The vector $\mathbf{v}_{\mathrm{F}}$ can be re-written in the $\mathcal{F}_2$ frame

$$\mathbf{v}_{\mathrm{F}} = \begin{bmatrix} V\cos\gamma + (\sigma + (l-d)\omega)\sin\gamma \\ -V\sin\gamma + (\sigma + (l-d)\omega)\cos\gamma \end{bmatrix}_{\mathcal{F}_2}, \tag{105}$$

which can also be obtained by substituting (97) into (6).

Using (103) the slip angle at the rear can be calculated as

$$\tan\alpha_{\mathrm{R}} = -\frac{v_{\mathrm{R}}^{y_1}}{v_{\mathrm{R}}^{x_1}} = -\frac{\sigma - d\omega}{V}. \tag{106}$$

At the front, we can use (104) to obtain

$$\tan\left(\alpha_{\mathrm{F}} - \gamma\right) = -\frac{v_{\mathrm{F}}^{y_1}}{v_{\mathrm{F}}^{x_1}} = -\frac{\sigma + (l-d)\omega}{V}, \tag{107}$$

or use (105) to obtain

$$\tan\alpha_{\mathrm{F}} = -\frac{v_{\mathrm{F}}^{y_2}}{v_{\mathrm{F}}^{x_2}} = -\frac{-V\sin\gamma + (\sigma + (l-d)\omega)\cos\gamma}{V\cos\gamma + (\sigma + (l-d)\omega)\sin\gamma}. \tag{108}$$

One may use trigonometric identities to show that the latter two definitions are identical. Finally the tire forces can be expressed as

$$\mathbf{F}_{\mathrm{R}} = \begin{bmatrix} 0 \\ F_{\mathrm{R}} \end{bmatrix}_{\mathcal{F}_1}, \qquad \mathbf{F}_{\mathrm{F}} = \begin{bmatrix} -F_{\mathrm{F}}\sin\gamma \\ F_{\mathrm{F}}\cos\gamma \end{bmatrix}_{\mathcal{F}_1}, \qquad \mathbf{F}_{\mathrm{F}} = \begin{bmatrix} 0 \\ F_{\mathrm{F}} \end{bmatrix}_{\mathcal{F}_2}. \tag{109}$$

Substituting (103)–(109) into (102), the virtual power becomes

$$\begin{aligned} \delta P &= F_{\mathrm{R}}\,\delta(\sigma - d\omega) - F_{\mathrm{F}}\sin\gamma\,\delta V + F_{\mathrm{F}}\cos\gamma\,\delta\left(\sigma + (l-d)\omega\right) + (M_{\mathrm{R}} + M_{\mathrm{F}})\,\delta\omega \\ &= (F_{\mathrm{R}} + F_{\mathrm{F}}\cos\gamma)\,\delta\sigma + (-d\,F_{\mathrm{R}} + (l-d)F_{\mathrm{F}}\cos\gamma + M_{\mathrm{R}} + M_{\mathrm{F}})\,\delta\omega, \end{aligned} \tag{110}$$

where we used that $\delta V = 0$. Reading the coefficients of the virtual pseudo velocities $\delta\sigma$ and $\delta\omega$ lead to the the pseudo forces

$$\begin{aligned} \Pi_{\sigma} &= F_{\mathrm{R}} + F_{\mathrm{F}}\cos\gamma, \\ \Pi_{\omega} &= -d\,F_{\mathrm{R}} + (l-d)F_{\mathrm{F}}\cos\gamma + M_{\mathrm{R}} + M_{\mathrm{F}}. \end{aligned} \tag{111}$$

Thus, (101) and (111) yield the Appell–Gibbs equations

$$\begin{aligned} \frac{\partial S}{\partial \dot{\sigma}} = \Pi_\sigma \quad &\Rightarrow \quad m\,(\dot{\sigma} + V\omega) = F_\mathrm{R} + F_\mathrm{F}\cos\gamma\,, \\ \frac{\partial S}{\partial \dot{\omega}} = \Pi_\omega \quad &\Rightarrow \quad J_\mathrm{G}\dot{\omega} = -d\,F_\mathrm{R} + (l-d)F_\mathrm{F}\cos\gamma + M_\mathrm{R} + M_\mathrm{F}. \end{aligned} \tag{112}$$

Combining these with the kinematic Eq. (97) gives the equations of motion

$$\begin{aligned} m\,(\dot{\sigma} + V\omega) &= F_\mathrm{R} + F_\mathrm{F}\cos\gamma, \\ J_\mathrm{G}\dot{\omega} &= -d\,F_\mathrm{R} + (l-d)F_\mathrm{F}\cos\gamma + M_\mathrm{R} + M_\mathrm{F}, \\ \dot{\psi} &= \omega, \\ \dot{x}_\mathrm{G} &= V\cos\psi - \sigma\sin\psi, \\ \dot{y}_\mathrm{G} &= V\sin\psi + \sigma\cos\psi. \end{aligned} \tag{113}$$

Here the lateral tire forces $F_\mathrm{R} = F_\mathrm{R}(\alpha_\mathrm{R})$, $F_\mathrm{F} = F_\mathrm{F}(\alpha_\mathrm{F})$ are given by (85), (86), the aligning moments $M_\mathrm{R} = M_\mathrm{R}(\alpha_\mathrm{R})$, $M_\mathrm{F} = M_\mathrm{F}(\alpha_\mathrm{F})$ are given by (93), (94), while the slip angles α_R, α_F are obtained from (106)–(108). The first two rows in (113) correspond to the lateral dynamics and the yaw dynamics, such that the torque equation is written about the center of mass G. Notice that these two equations are decoupled from the remaining three; the former ones are often referred to as the essential dynamics, while the latter ones are referred to as the hidden dynamics. Indeed, when the position and the yaw angle are fed back through a control law, the essential and hidden dynamics become coupled.

Similar to the model with rigid wheels, we may choose the position $(x_\mathrm{R}, y_\mathrm{R})$ of the rear axle center point R as configuration coordinates. Accordingly, we shall use

$$\dot{x}_\mathrm{R}\cos\psi + \dot{y}_\mathrm{R}\sin\psi = V\,, \tag{114}$$

instead of the kinematic constraint (95) and choose the lateral velocity of point R, denoted by $\hat{\sigma}$, and the yaw rate ω as pseudo velocities:

$$\begin{aligned} \hat{\sigma} &= -\dot{x}_\mathrm{R}\sin\psi + \dot{y}_\mathrm{R}\cos\psi, \\ \omega &= \dot{\psi}, \end{aligned} \tag{115}$$

instead of (96). The corresponding derivation is carried out in Appendix 7.

Finally, we remark that the above vehicle models with tires describe rear wheel drive (RWD) vehicles, as restricting the longitudinal velocity is equivalent to restricting the speed of the rear axle center point R. Similar to the models with rigid wheels, one may also derive models for front wheel drive (FWD) vehicles by restricting the wheel directional velocity component of the point F. When carrying out the related calculations, one shall use the kinematic constraint

$$\dot{x}_\mathrm{G}\cos(\psi+\gamma) + \dot{y}_\mathrm{G}\sin(\psi+\gamma) + (l-d)\dot{\psi}\sin\gamma = \hat{V}, \tag{116}$$

cf. (17), instead of (95). Also, one shall use the kinematic constraint

$$\dot{x}_{\mathrm{R}} \cos(\psi + \gamma) + \dot{y}_{\mathrm{R}} \sin(\psi + \gamma) + l\dot{\psi} \sin\gamma = \hat{V}, \tag{117}$$

cf. (18), instead of (114). Interested readers may find more details about these models and experimentation in Oh et al. (2021).

4.1.1 Steady State Cornering

Consider the steady state cornering of the vehicle while using the constant input $\gamma(t) \equiv \gamma_*$. Then substituting the steady state $\sigma(t) \equiv \sigma_*$, $\omega(t) \equiv \omega_*$ into the first two equations of (113) yields

$$\begin{aligned} mV\omega_* &= F_{\mathrm{R}}^* + F_{\mathrm{F}}^* \cos\gamma_*, \\ 0 &= -d\, F_{\mathrm{R}}^* + (l-d) F_{\mathrm{F}}^* \cos\gamma_* + M_{\mathrm{R}}^* + M_{\mathrm{F}}^*, \end{aligned} \tag{118}$$

where the lateral tire forces $F_{\mathrm{R}}^* = F_{\mathrm{R}}(\alpha_{\mathrm{R}}^*)$, $F_{\mathrm{F}}^* = F_{\mathrm{F}}(\alpha_{\mathrm{F}}^*)$ and aligning moments $M_{\mathrm{R}}^* = M_{\mathrm{R}}(\alpha_{\mathrm{R}}^*)$, $M_{\mathrm{F}}^* = M_{\mathrm{F}}(\alpha_{\mathrm{F}}^*)$ are calculated from (85), (86) and (93), (94), respectively. The steady state slip angles $\alpha_{\mathrm{R}}^*, \alpha_{\mathrm{F}}^*$ are obtained from

$$\tan\alpha_{\mathrm{R}}^* = -\frac{\sigma_* - d\omega_*}{V}, \qquad \tan\left(\alpha_{\mathrm{F}}^* - \gamma_*\right) = -\frac{\sigma_* + (l-d)\omega_*}{V}, \tag{119}$$

cf. (106), (107). One may solve (numerically) the nonlinear algebraic Eqs. (118) and (119) for the steady state lateral velocity σ_* and the steady state yaw rate ω_*. Then integrating the last three rows of (113) results in

$$\begin{aligned} \psi(t) &= \omega_* t + \psi_0, \\ x_{\mathrm{G}}(t) &= \frac{V}{\omega_*} \sin(\omega_* t + \psi_0) + \frac{\sigma_*}{\omega_*} \cos(\omega_* t + \psi_0) + x_{\mathrm{C}}, \\ y_{\mathrm{G}}(t) &= -\frac{V}{\omega_*} \cos(\omega_* t + \psi_0) + \frac{\sigma_*}{\omega_*} \sin(\omega_* t + \psi_0) + y_{\mathrm{C}}, \end{aligned} \tag{120}$$

where $\psi_0 = \psi(0)$ while x_{C} and y_{C} come from the initial conditions. Again, these formulae describe the circular motion about the instantaneous center of rotation C as shown in Fig. 16, while the radius of curvature of the center of mass G is

$$\rho_{\mathrm{G}} = \sqrt{(x_{\mathrm{G}} - x_{\mathrm{C}})^2 + (y_{\mathrm{G}} - y_{\mathrm{C}})^2} = \frac{\sqrt{V^2 + \sigma_*^2}}{|\omega_*|}. \tag{121}$$

Similarly for the rear axle center point R one may use (194) to obtain the steady state values $\hat{\sigma}_*, \omega_*$ and derive

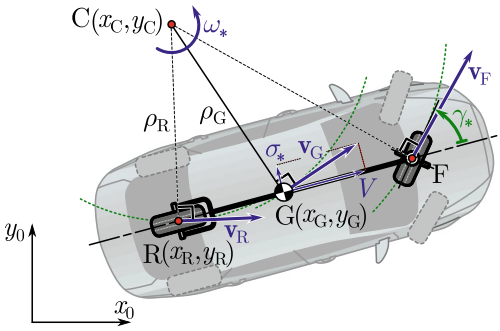

Fig. 16 Steady state cornering for a bicycle model with elastic tires. The instantaneous center or rotation C and the radii of curvature for points G and R are indicated

$$\begin{aligned}
\psi(t) &= \omega_* t + \psi_0,\\
x_R(t) &= \frac{V}{\omega_*}\sin(\omega_* t + \psi_0) + \frac{\hat{\sigma}_*}{\omega_*}\cos(\omega_* t + \psi_0) + x_C,\\
y_R(t) &= -\frac{V}{\omega_*}\cos(\omega_* t + \psi_0) + \frac{\hat{\sigma}_*}{\omega_*}\sin(\omega_* t + \psi_0) + y_C,
\end{aligned} \tag{122}$$

cf. (120). These result in the radius of curvature of the rear axle center point R:

$$\rho_R = \sqrt{(x_R - x_C)^2 + (y_R - y_C)^2} = \frac{\sqrt{V^2 + \hat{\sigma}_*^2}}{|\omega_*|}, \tag{123}$$

cf. (121). Also, using (120) and (122), and exploiting that $\sigma = \hat{\sigma} + d\,\omega$ one may show that $(x_G - x_R)^2 + (y_G - y_R)^2 = d^2$, justifying why the constants x_C and y_C need to be the same in both formulae.

Note that in general, the nonlinear algebraic Eqs. (118), (119) can only be solved numerically. However, by assuming small angles, the following simplifications can be made

$$\sin\gamma_* \approx \gamma_*\,,\quad \cos\gamma_* \approx 1,\quad \tan\alpha_R^* \approx \alpha_R^*,\quad \tan\left(\alpha_F^* - \gamma_*\right) \approx \alpha_F^* - \gamma_*\,. \tag{124}$$

Then (119) simplifies to

$$\alpha_R^* \approx -\frac{\sigma_* - d\omega_*}{V},\qquad \alpha_F^* - \gamma_* = -\frac{\sigma_* + (l-d)\omega_*}{V}, \tag{125}$$

while the force characteristics (85), (86) and the aligning moments (93), (94) simplify to

$$\begin{aligned}
F_R^* &\approx C_R\alpha_R^*, \qquad F_F^* \approx C_F\alpha_F^*,\\
M_R^* &\approx -\frac{a}{3}C_R\alpha_R^*, \quad M_F^* \approx -\frac{a}{3}C_F\alpha_F^*.
\end{aligned} \tag{126}$$

Since the aligning moments are much smaller in magnitude than the torques $d\,F_{\mathrm{R}}^{*}$ and $(l-d)F_{\mathrm{F}}^{*}$ in (118), they are often neglected yielding

$$\begin{aligned} mV\omega_{*} &\approx C_{\mathrm{R}}\alpha_{\mathrm{R}}^{*} + C_{\mathrm{F}}\alpha_{\mathrm{F}}^{*}, \\ 0 &\approx -d\,C_{\mathrm{R}}\alpha_{\mathrm{R}}^{*} + (l-d)C_{\mathrm{F}}\alpha_{\mathrm{F}}^{*}. \end{aligned} \tag{127}$$

Then the linear algebraic Eqs. (125), (127) can be solved for σ_{*}, ω_{*}, α_{R}^{*}, α_{F}^{*}.

One may express from (125) that the difference between the front and the rear slip angles is

$$\alpha_{\mathrm{F}}^{*} - \alpha_{\mathrm{R}}^{*} \approx \gamma_{*} - \frac{l\,\omega_{*}}{V}. \tag{128}$$

If the two slip angles are the same $\alpha_{\mathrm{F}}^{*} = \alpha_{\mathrm{R}}^{*}$, then we talk about a neutral steer vehicle. In this case, we have $\omega_{*} \approx \frac{V}{l}\gamma_{*}$ which is the small angle approximation of (19). That is, in terms of how much yaw rate is generated by a given steering angle, the vehicle behaves like the kinematic model (in steady state for small steering angles). Nevertheless, the trajectory of the vehicle moves on a different trajectory compared to the kinematic model as only the difference between the slip angles is zero, rather than the slip angles themselves being zero. If $\alpha_{\mathrm{F}}^{*} > \alpha_{\mathrm{R}}^{*}$, we call it an understeer vehicle, which exerts less yaw rate for a given steering angle compared to the kinematic model. Finally, if $\alpha_{\mathrm{F}}^{*} < \alpha_{\mathrm{R}}^{*}$ we refer to it as an oversteer vehicle, which exerts more yaw rate compared to the kinematic model.

One may also express the difference of the slip angles from (127) as

$$\alpha_{\mathrm{F}}^{*} - \alpha_{\mathrm{R}}^{*} \approx \underbrace{\left(\frac{mgd}{lC_{\mathrm{F}}} - \frac{mg(l-d)}{lC_{\mathrm{R}}}\right)}_{:=K_{\mathrm{us}}} \frac{V\omega_{*}}{g}, \tag{129}$$

where K_{us} is the understeer coefficient (that is positive for understeer, zero for neutral steer, and negative for oversteer vehicles), while $V\omega_{*}/g$ is the steady state lateral acceleration at the center of gravity measured in g. Note that neutral steer can be achieved with a 50–50 weight ratio (i.e., $d = l - d$) and using the same type of tires at the front and at the rear ($C_{\mathrm{F}} = C_{\mathrm{R}}$).

Combining (128) and (129) one may obtain the steady state yaw rate

$$\omega_{*} \approx \frac{V\gamma_{*}}{l + K_{\mathrm{us}}\dfrac{V^{2}}{g}}. \tag{130}$$

Also, eliminating α_{F}^{*} from (127) and using α_{R}^{*} from (125) leads to

$$\sigma_{*} \approx \left(d - \frac{m(l-d)V^{2}}{C_{\mathrm{R}}l}\right)\omega^{*}. \tag{131}$$

Using these in (121) one may obtain the radius of curvature

$$\rho_{\mathrm{G}} \approx \sqrt{\frac{1}{\gamma_*^2}\left(l + K_{\mathrm{us}}\frac{V^2}{g}\right)^2 + \left(d - \frac{m(l-d)V^2}{C_{\mathrm{R}}l}\right)^2}. \tag{132}$$

For small steering angles, the first term typically dominates over the second term under the square root, so the second one is often omitted. Then, the velocity dependence of the radius is driven by the understeer/oversteer coefficient K_{us}. For neutral steer vehicles (i.e., for $K_{\mathrm{us}} = 0$) this speed dependence disappears, yielding $\rho_{\mathrm{G}} \approx \frac{l}{|\gamma_*|}$ which is the small angle approximation of (22) that was derived for the kinematic models. That is, understeer vehicles behave similarly to the rigid tire models in terms of the radius of curvature too. We emphasize that these arguments only hold under the small angle approximation (124), which may not be valid in many scenarios.

Neutral steer is somewhat difficult to achieve for automobiles with internal combustion engines, since having the engines at the front typically makes the car front heavy. This requires many design compromises if one wishes to achieve 50–50 weight ratio. For electric vehicles, neutral steer can be achieved by evenly distributing the battery packs, and that is the current trend followed in the industry.

Figure 17 highlights the difference between the steady state cornering solution of the bicycle model (10) with rigid wheels (dashed lines) and the bicycle model (113) with elastic tires (solid lines). Both numerical simulations are started at the initial position and orientation of $x_{\mathrm{G}}(0) = 0\,\mathrm{m}$, $y_{\mathrm{G}}(0) = 0\,\mathrm{m}$ and $\psi(0) = 0°$, but to avoid transient dynamics, the steady state values of the pseudo velocities (given by (118), (119)) are used as initial conditions in the more complex model ($\sigma(0) = \sigma_*$, $\omega(0) = \omega_*$). This different velocity state causes the vehicle trajectory to cross the

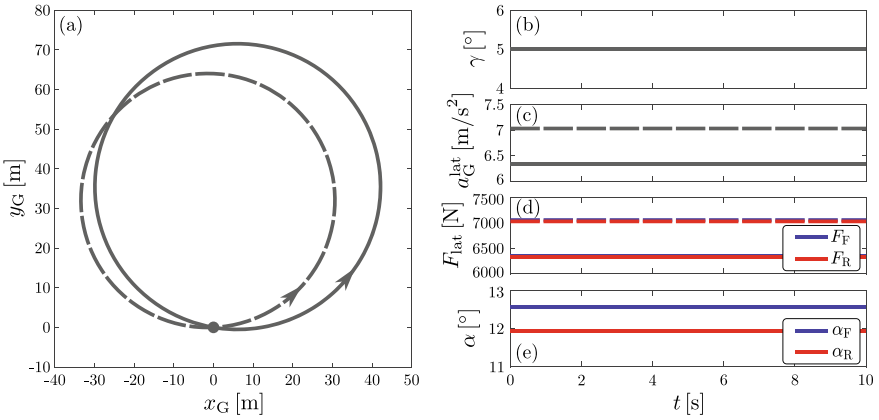

Fig. 17 Numerical simulation of steady state cornering of the bicycle model (113) with elastic tires at $V = 15\,\mathrm{m/s}$ with steering angle $\gamma = 5°$. **a** Trajectory of the center of mass G; **b** steering angle; **c** lateral acceleration of point G; **d** lateral tire forces at the front and rear wheels; **e** tire slip angles. Dashed lines show the corresponding quantities using the model with rigid wheels (10)

origin in a different direction [see panel (a)], and the radius of curvature is also larger due to the elasticity of the tires (cf. (22) and (121)). Due to the larger radius of curvature, the steady state lateral acceleration is smaller compared to the rigid wheel model [panel (c)], while the lateral tire forces [panel (d)] are also smaller than the constraining forces in the rigid wheel model, corresponding to the non-zero slip angles [shown in panel (e)].

We remark that the steady state radius of curvature of the rigid wheel model does not depend on the vehicle speed (the constraining forces are always assumed to be available to ensure the no side-slip condition), while higher speeds lead to larger slip angles in the dynamic model, resulting in larger radii of curvature.

4.1.2 Transient Dynamics

Figure 18 shows a lane-change maneuver with the control law

$$\gamma = -k_y y_{\mathrm{R}} - k_\psi \psi \,, \tag{133}$$

(originally introduced in (24)) for the bicycle model (113) with elastic tires. The vehicle trajectory is plotted in panel (a), while panel (b) shows the corresponding steering input. The kinematic quantities in panels (c)–(e) (lateral velocity, yaw rate

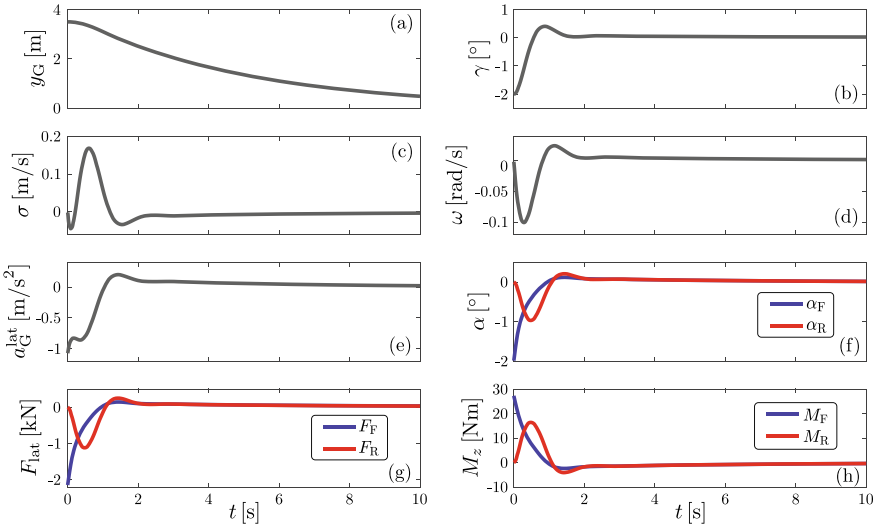

Fig. 18 Numerical simulation of a lane-change maneuver of the bicycle model (113) with elastic tires at $V = 15$ m/s while utilizing the control law (133) with gains $k_y = 0.01\,\mathrm{m}^{-1}$ and $k_\psi = 0.8$. **a** Lateral position of the center of mass G; **b** steering angle; **c** lateral velocity of point G; **d** vehicle yaw rate; **e** lateral acceleration of point G; **f** tire slip angles; **g** lateral tire forces; **h** aligning moments

and lateral acceleration, respectively) show that the lane change is performed in a smooth manner, without sudden movements that might cause passenger discomfort.

Since there are no steering dynamics involved, the steering angle calculated from (133) shows up instantaneously at the wheels. Panels (f)–(h) show the resulting slip angles, tire forces and aligning moments. Once the transient dynamics die down and the vehicle reaches the steady state of straight-line motion along the reference path, these all return to zero.

4.2 *Bicycle Model with Elastic Tires and Steering Dynamics*

Here we consider the vehicle with elastic tires while adding the steering dynamics as illustrated in Fig. 19.

That is, the front wheel is steered by the internal steering torque T_s, while the longitudinal speed is still restricted. Thus, we have four generalized coordinates: the position (x_G, y_G), the yaw angle ψ, and the steering angle γ. Considering that we have one kinematic constraint (95), we need to select $4 - 1 = 3$ pseudo velocities. As before, we choose the lateral velocity σ of point G and the yaw rate ω, see (96), and we also add the steering rate

$$\Omega := \dot{\gamma}, \tag{134}$$

as previously for the vehicle with rigid wheels, cf. (25). This results in $4 - \frac{1}{2} = 3.5$ degrees of freedom overall.

Equations (95), (96), and (134) can be solved for the generalized velocities:

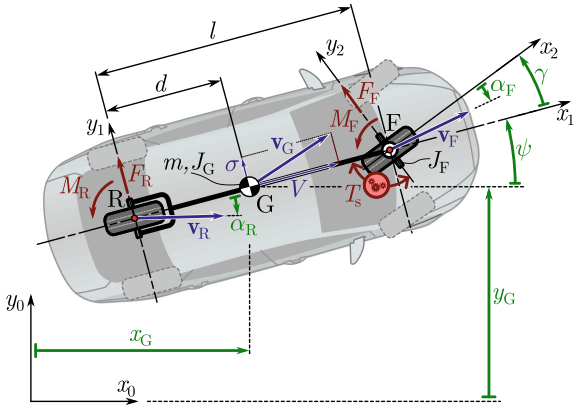

Fig. 19 Single track model of an automobile with elastic tires and steering dynamics

$$\begin{aligned} \dot{x}_\mathrm{G} &= V\cos\psi - \sigma\sin\psi, \\ \dot{y}_\mathrm{G} &= V\sin\psi + \sigma\cos\psi, \\ \dot{\psi} &= \omega, \\ \dot{\gamma} &= \Omega, \end{aligned} \tag{135}$$

and taking the time derivative results in

$$\begin{aligned} \ddot{x}_\mathrm{G} &= -V\omega\sin\psi - \dot{\sigma}\sin\psi - \sigma\omega\cos\psi, \\ \ddot{y}_\mathrm{G} &= V\omega\cos\psi + \dot{\sigma}\cos\psi - \sigma\omega\sin\psi\,, \\ \ddot{\psi} &= \dot{\omega}, \\ \ddot{\gamma} &= \dot{\Omega}. \end{aligned} \tag{136}$$

These allow us to construct the acceleration energy of the system, which consists of the vehicle body and the steering system:

$$\begin{aligned} S &= \frac{1}{2}m\left(\ddot{x}_\mathrm{G}^2 + \ddot{y}_\mathrm{G}^2\right) + \frac{1}{2}J_\mathrm{G}\ddot{\psi}^2 + \frac{1}{2}J_\mathrm{F}\left(\ddot{\psi} + \ddot{\gamma}\right)^2 + \ldots \\ &= \frac{1}{2}m\left(\dot{\sigma}^2 + 2V\omega\dot{\sigma}\right) + \frac{1}{2}J_\mathrm{G}\dot{\omega}^2 + \frac{1}{2}J_\mathrm{F}\left(\dot{\omega} + \dot{\Omega}\right)^2 + \ldots, \end{aligned} \tag{137}$$

where m is the mass of the vehicle, J_G and J_F are the mass moments of inertia of the vehicle and the steering system, respectively, while the terms that do not contain the pseudo accelerations $\dot{\sigma}$, $\dot{\omega}$, $\dot{\Omega}$ are incorporated in $\ldots$. The virtual power of the system rises from the tire forces and moments and also from the steering torque

$$\begin{aligned} \delta P = {} & \left(F_\mathrm{R} + F_\mathrm{F}\cos\gamma\right)\delta\sigma + \left(-d\,F_\mathrm{R} + (l-d)F_\mathrm{F}\cos\gamma + M_\mathrm{R} + M_\mathrm{F}\right)\delta\omega \\ & + \left(M_\mathrm{F} + T_\mathrm{s}\right)\delta\Omega, \end{aligned} \tag{138}$$

cf. (29) and (110). The coefficients of the virtual velocities $\delta\sigma$, $\delta\omega$ and $\delta\Omega$ yield the pseudo forces

$$\begin{aligned} \Pi_\sigma &= F_\mathrm{R} + F_\mathrm{F}\cos\gamma, \\ \Pi_\omega &= -d\,F_\mathrm{R} + (l-d)F_\mathrm{F}\cos\gamma + M_\mathrm{R} + M_\mathrm{F}, \\ \Pi_\Omega &= M_\mathrm{F} + T_\mathrm{s}. \end{aligned} \tag{139}$$

Then, (137) and (139) result in the Appell–Gibbs equations

$$\begin{aligned} \frac{\partial S}{\partial\dot{\sigma}} = \Pi_\sigma \quad &\Rightarrow \quad m\left(\dot{\sigma} + V\omega\right) = F_\mathrm{R} + F_\mathrm{F}\cos\gamma\,, \\ \frac{\partial S}{\partial\dot{\omega}} = \Pi_\omega \quad &\Rightarrow \quad J_\mathrm{G}\dot{\omega} + J_\mathrm{F}(\dot{\omega} + \dot{\Omega}) = -d\,F_\mathrm{R} + (l-d)F_\mathrm{F}\cos\gamma + M_\mathrm{R} + M_\mathrm{F}, \\ \frac{\partial S}{\partial\dot{\Omega}} = \Pi_\Omega \quad &\Rightarrow \quad J_\mathrm{F}(\dot{\omega} + \dot{\Omega}) = M_\mathrm{F} + T_\mathrm{s}. \end{aligned} \tag{140}$$

Rearranging these and combining them with the kinematic Eq. (135) lead to the equations of motion

$$
\begin{aligned}
m\,(\dot{\sigma} + V\omega) &= F_{\mathrm{R}} + F_{\mathrm{F}} \cos\gamma, \\
J_{\mathrm{G}}\dot{\omega} &= -d\,F_{\mathrm{R}} + (l-d)F_{\mathrm{F}} \cos\gamma + M_{\mathrm{R}} - T_{\mathrm{s}}, \\
J_{\mathrm{F}}\dot{\Omega} &= M_{\mathrm{F}} + T_{\mathrm{s}} - \frac{J_{\mathrm{F}}}{J_{\mathrm{G}}}\left(-d\,F_{\mathrm{R}} + (l-d)F_{\mathrm{F}} \cos\gamma + M_{\mathrm{R}} - T_{\mathrm{s}}\right), \\
\dot{\gamma} &= \Omega, \\
\dot{\psi} &= \omega, \\
\dot{x}_{\mathrm{G}} &= V\cos\psi - \sigma\sin\psi, \\
\dot{y}_{\mathrm{G}} &= V\sin\psi + \sigma\cos\psi.
\end{aligned}
\tag{141}
$$

Here the lateral tire forces $F_{\mathrm{R}} = F_{\mathrm{R}}(\alpha_{\mathrm{R}})$, $F_{\mathrm{F}} = F_{\mathrm{F}}(\alpha_{\mathrm{F}})$ and the aligning moments $M_{\mathrm{R}} = M_{\mathrm{R}}(\alpha_{\mathrm{R}})$, $M_{\mathrm{F}} = M_{\mathrm{F}}(\alpha_{\mathrm{F}})$ are still given by (85), (86) and (93), (94), respectively, while the slip angles $\alpha_{\mathrm{R}}, \alpha_{\mathrm{F}}$ are still obtained from (106)–(108). The first four rows in (141) describe the essential dynamics and these are decoupled from the last three equations, which describe the hidden dynamics. However, the essential and hidder dynamics become coupled when feeding back the position and the yaw angle via control.

The term with coefficient $J_{\mathrm{F}}/J_{\mathrm{G}}$ in the third equation may be omitted since J_{F} is much smaller J_{G}. On the other hand, as M_{F} and T_{s} are typically of the same order of magnitude, the aligning moment has an important role in the vehicle model when the steering dynamics is considered. The steering torque can still be calculated as

$$
T_{\mathrm{s}} = k_{\mathrm{t}}\left(\gamma_{\mathrm{d}} - \gamma\right), \tag{142}
$$

cf. (35), where γ_{d} is the desired steering angle and k_{t} is the torsional stiffness of the steering system or the proportional gain of the steer-by-wire system. In this case, instead of setting the steering angle directly as in (133), we assign the desired steering angle

$$
\gamma_{\mathrm{d}} = -k_y y_{\mathrm{R}} - k_\psi \psi, \tag{143}
$$

cf. (36).

Again, we may choose the position $(x_{\mathrm{R}}, y_{\mathrm{R}})$ of the rear axle center point R as configuration coordinates, use the kinematic constraint (114), and choose the lateral velocity $\hat{\sigma}$ of point R, the yaw rate ω and the steering rate Ω as pseudo velocities according to (115) and (134). The detailed derivation is carried out in Appendix 7.

Finally, we remark that one may also derive models for front wheel drive (FWD) vehicles with steering dynamics by restricting the wheel directional velocity component of the point F. In order to do this, one shall use (116) instead of (95), and one shall use (117) instead of (114) during the derivation. More details about such models and corresponding experimentation can be found in Beregi et al. (2023), Vörös et al. (2023b).

4.2.1 Steady State Cornering

When considering a constant desired steering angle $\gamma_{\mathrm{d}}(t) = \gamma_{\mathrm{d}}^*$, the steady state cornering solution of the models (141) and (202) with elastic tires and steering dynamics are still given in the forms (120) and (122), respectively, and the corresponding radii of curvature are in the forms (121) and (123), respectively. However, the steady state lateral velocity $\sigma(t) \equiv \sigma_*$, yaw rate $\omega(t) \equiv \omega_*$ and steering angle $\gamma(t) \equiv \gamma_*$ are now given by

$$\begin{aligned} mV\omega_* &= F_{\mathrm{R}}^* + F_{\mathrm{F}}^* \cos\gamma_*, \\ 0 &= -d\, F_{\mathrm{R}}^* + (l-d) F_{\mathrm{F}}^* \cos\gamma_* + M_{\mathrm{R}}^* - T_{\mathrm{s}}^*, \\ 0 &= M_{\mathrm{F}}^* + T_{\mathrm{s}}^*, \\ T_{\mathrm{s}}^* &= k_{\mathrm{t}} \left(\gamma_{\mathrm{d}}^* - \gamma_*\right), \end{aligned} \tag{144}$$

rather than by (118). Here the tire forces $F_{\mathrm{R}}^* = F_{\mathrm{R}}(\alpha_{\mathrm{R}}^*)$, $F_{\mathrm{F}}^* = F_{\mathrm{F}}(\alpha_{\mathrm{F}}^*)$ and moments $M_{\mathrm{R}}^* = M_{\mathrm{R}}(\alpha_{\mathrm{R}}^*)$, $M_{\mathrm{F}}^* = M_{\mathrm{F}}(\alpha_{\mathrm{F}}^*)$ are calculated from (85), (86) and (93), (94), respectively, while the steady state slip angles α_{R}^*, α_{F}^* are obtained from (119).

We emphasize that since, in general, $\gamma_* \neq \gamma_{\mathrm{d}}^*$, the numerical value of the radius of curvature differs from the values obtained when the steering dynamics was neglected. This effect can only be observed in the case of elastic tires since the aligning moments are zeros for rigid wheels.

Considering the small angle approximations in (124) and (126), we obtain

$$\begin{aligned} mV\omega_* &\approx C_{\mathrm{R}}\alpha_{\mathrm{R}}^* + C_{\mathrm{F}}\alpha_{\mathrm{F}}^*, \\ 0 &\approx -d\, C_{\mathrm{R}}\alpha_{\mathrm{R}}^* + (l-d) C_{\mathrm{F}}\alpha_{\mathrm{F}}^* - C_{\mathrm{R}}\frac{a}{3}\alpha_{\mathrm{R}}^* - C_{\mathrm{F}}\frac{a}{3}\alpha_{\mathrm{F}}^*, \\ 0 &\approx -C_{\mathrm{F}}\frac{a}{3}\alpha_{\mathrm{F}}^* + k_{\mathrm{t}}\left(\gamma_{\mathrm{d}}^* - \gamma_*\right). \end{aligned} \tag{145}$$

These together with (125) form a system of linear algebraic equations for σ_*, ω_*, γ_*, α_{R}^*, α_{F}^* and further emphasize the necessity of including the aligning moments in the model when the steering dynamics are considered.

Figure 20 shows a comparison between the steady state cornering solutions of the bicycle models with rigid wheels (10), (33) (dashed lines), the model with tire dynamics but without steering dynamics (113) (dotted lines), and the model with both tire and steering dynamics (141), (142) (solid lines). While the difference between the rigid wheel models and the dynamic model without steering dynamics is due to the elasticity of the tires and the resulting slip angles (as detailed at the end of Sect. 4.1), Fig. 20b shows that there is a steady state error between the desired and the realized steering angle when both tire and steering dynamics are considered. The steering dynamics described by the third row in (141) show that this difference is due to the aligning moment of the front tires. Therefore, even though these moments are often neglected due to their negligible impact on the dynamics of the vehicle body, they greatly affect the steering dynamics.

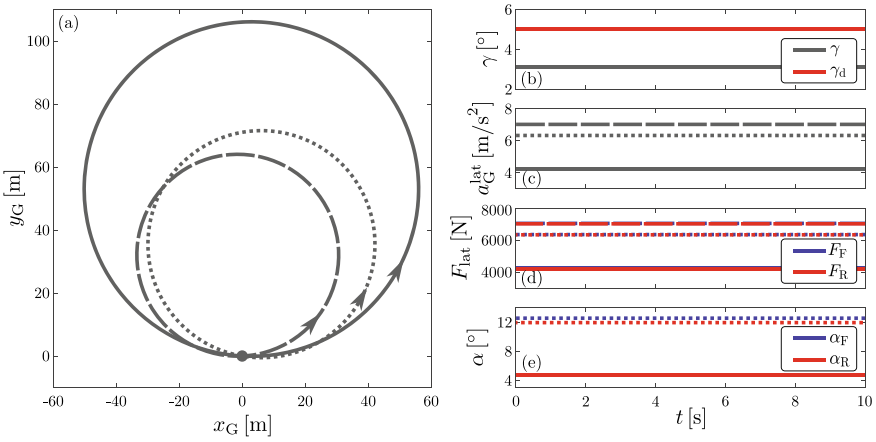

Fig. 20 Numerical simulation of steady state cornering of the bicycle model with elastic tires and steering dynamics (141), (142) at $V = 15\,\text{m/s}$ with desired steering angle $\gamma_d = 5°$. **a** Trajectory of the center of mass G; **b** desired (red) and realized (black) steering angle; **c** lateral acceleration of point G; **d** lateral tire forces at the front and rear wheels; **e** tire slip angles. Dashed lines show the corresponding quantities using the model with rigid wheel (10), while dotted lines indicate the results using the bicycle model with elastic tires but without steering dynamics (113)

The steady state error in Fig. 20b can be adjusted by tuning the stiffness k_t, or in case of steer-by-wire system, by designing a more advanced controller than (142). In the scenario depicted in Fig. 20, the smaller realized steering angle causes the vehicle to follow a path with a larger radius compared to the other two models [see panel (a)], resulting in smaller lateral acceleration [panel (c)], tire forces [panel (d)] and slip angles [panel (e)].

4.2.2 Transient Dynamics

The steering system also affects the lane-change maneuver as shown in Fig. 21: similarly to the rigid wheel model in Fig. 9, strong transient oscillations appear in the steering angle when considering the model with tire and steering dynamics (141), (142) when using the control law (143) (see Fig. 21b). Although these oscillations do not influence the vehicle trajectory significantly [panel (a)], they carry over into the kinematic quantities in panels (c)–(e) and into the dynamics of the front tires in panels (f)–(h), affecting both passenger comfort and tire wear.

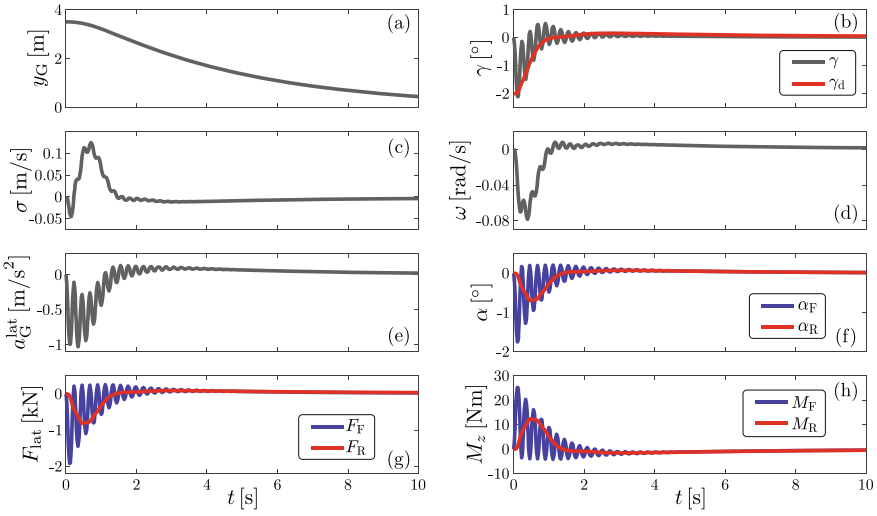

Fig. 21 Numerical simulation of a lane-change maneuver of the bicycle model with elastic tires and steering dynamics (141) and (142) at $V = 15$ m/s while utilizing the control law (143) with gains $k_y = 0.01\,\mathrm{m}^{-1}$ and $k_\psi = 0.8$. **a** Lateral position of the center of mass G; **b** desired (red) and realized (black) steering angle; **c** lateral velocity of point G; **d** vehicle yaw rate; **e** lateral acceleration of point G; **f** tire slip angles; **g** lateral tire forces; **h** aligning moments

5 Conclusion

In this book chapter, we presented single track models of different complexity for the handling dynamics of automobiles while considering different assumptions regarding the tire-road contact. For simplicity, we started with models assuming rigid wheels with zero side slip angles, where the kinematic constraints determined the equation of motion. For such kinematic models, the tire-ground contact forces are as large as necessary to maintain the constraints. The main advantage of these models is their simplicity, which makes them look attractive for control design. On the other hand, the rigid wheel assumption is typically only reasonable at low-speed maneuvers.

By taking into account the elasticity of the tires, we developed a brush tire model where the lateral tire forces and the aligning moments were calculated based on the tire deformations, in particular, based on the slip angles in quasi-stationary scenarios. These models have higher fidelity but also have higher complexity as they contain many vehicle parameters, and some of those may need to be estimated if one wants to use the models for control design. Numerical simulations were carried out to compare the steady state cornering behavior of the different models and also their transient behavior in a lane change maneuver. We demonstrated that both tire elasticity and steering compliance can influence the handling dynamics of the vehicle.

The equations of motion for all models were derived using the Appellian approach which enabled us to handle kinematic constraints and to present the equations of

motion in the most simplistic form. Using this approach also allowed us to reveal the connections between the different models. In addition, it may accommodate more advanced tire models like the delayed tire model (Takács and Stépán, 2013), can be used to derive dual-track vehicle models (Mi et al., 2020) and vehicles with trailers (Beregi et al., 2016) without exploding the model complexity. Moreover, the developed models can be analyzed with the help of bifurcation analysis to reveal the stable and unstable motions that govern the dynamics (Mastinu et al., 2023; Oh et al., 2021; Steindl et al., 2023; Vörös et al., 2023a, b).

6 Appell–Gibbs Equations

Here we briefly review the concepts involved in nonholonomic systems. We start with defining constraints and degrees of freedom, and then derive the Appell–Gibbs equations, which are used extensively in the main part of the manuscript. For the sake of simplicity, the derivations are carried out for systems of particles and we provide the necessary formulas to allow the reader to generalize the calculations for rigid bodies. The reader may refer to Baruh (1999), Bloch (2003), De Sapio (2017), Gantmacher (1970), Greenwood (2003), Kane and Levinson (1985), Koon and Marsden (1997), Limebeer and Massaro (2018), Neimark and Fufaev (1972), Ostrovskaya and Angeles (1998), Papastavridis (2002) for more details on dynamics of nonholonomic systems.

Consider a system of N particles of mass m_i, $i = 1, \ldots, N$ as shown in Fig. 22. Without constraints, this system has $3N$ degrees of freedom, that is, it requires $3N$ scalar coordinates to unambiguously describe the system. The corresponding Newtonian equations of motion can be formulated as $3N$ second-order ordinary differential equations, or equivalently, $6N$ first-order ordinary differential equations. In particular, one may use the position vectors $\mathbf{r}_i$, $i = 1, \ldots, N$ of the particles to describe their motion uniquely.

6.1 Geometric and Kinematic Constraints

Now consider that the system is subject to g geometric (also called holonomic) constraints of the form

$$f_\alpha(\mathbf{r}_i, t) = 0, \quad \alpha = 1, \ldots, g, \tag{146}$$

see the examples f_1 and f_2 in Fig. 22. Here we use a simplified notation so that $\mathbf{r}_i$ stands for $\mathbf{r}_1, \ldots, \mathbf{r}_N$ representing that each constraint may depend on the position vectors of all particles as well as on the time t explicitly. This notation is implemented in order to keep the complexity of formulas manageable. For example, $w_\beta(\mathbf{r}_j, t)$ means that w_β may depend on $\mathbf{r}_1, \ldots, \mathbf{r}_N$. Assume that apart from the geometric

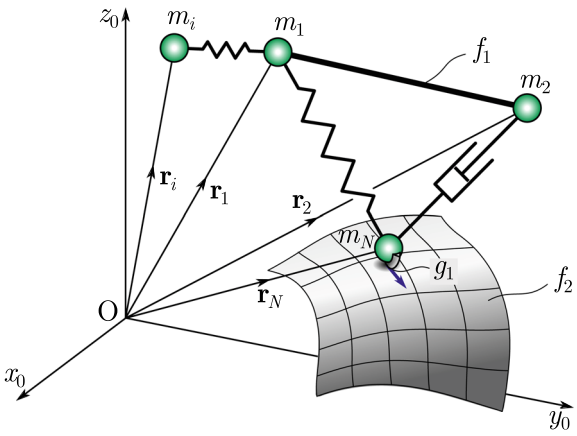

Fig. 22 Dynamical system of N particles with constraints. A rod maintains the distance l between particles m_1 and m_2, which is described by the constraint f_1. The particle m_N is constrained to a surface while its velocity is directed by the blade of a skate sliding on the surface; the corresponding constraining equations are given by f_2 and g_1, respectively

constraints, we also have h kinematic (also called nonholonomic) constraints of the form

$$g_\beta(\mathbf{r}_i, \dot{\mathbf{r}}_i, t) = 0, \quad \beta = 1, \ldots, h, \tag{147}$$

where the dot represents derivative with respect to time t; see the example g_1 in Fig. 22.

We show that the geometric constraints can be eliminated using generalized coordinates, while the kinematic constrains can be handled using pseudo velocities, although (147) shall be kept as part of the equations of motion. Consequently, one can define the degrees of freedom of the system as $3N - g - h/2$ corresponding to the $6N - 2g - h$ first-order ordinary differential equations that govern the motion of the system; see also Hu (2018).

In order to simplify the matter, we only consider kinematic constraints that are affine functions of velocities $\dot{\mathbf{r}}_i$:

$$\sum_{i=1}^{N} \mathbf{w}_{\beta i}(\mathbf{r}_j, t) \cdot \dot{\mathbf{r}}_i + w_\beta(\mathbf{r}_j, t) = 0, \quad \beta = 1, \ldots, h, \tag{148}$$

where $\cdot$ denotes the dot product of vectors. All the sliding and/or rolling constraints considered in this book chapter can be written in the form (148) which seems to be quite generic in classical multi-body systems.

Before trying to eliminate the constraints, we list some definitions. As already indicated above, the actual velocity of particle i is denoted by $\dot{\mathbf{r}}_i$; this will be the solution of the equations of motion once they are constructed. The set of velocities that satisfy the constraints above (but may not satisfy the equations of motion) are called admissible velocities and they are denoted by $\{\dot{\mathbf{r}}_i^{\wedge}, \dot{\mathbf{r}}_i^{\wedge\wedge}, \dot{\mathbf{r}}_i^{\wedge\wedge\wedge}, \ldots\}$. One of these velocities is, in fact, the actual velocity. Finally, the virtual velocity is defined as the difference of two admissible velocities, e.g., $\delta\dot{\mathbf{r}}_i = \dot{\mathbf{r}}_i^{\wedge} - \dot{\mathbf{r}}_i^{\wedge\wedge}$; see illustrations

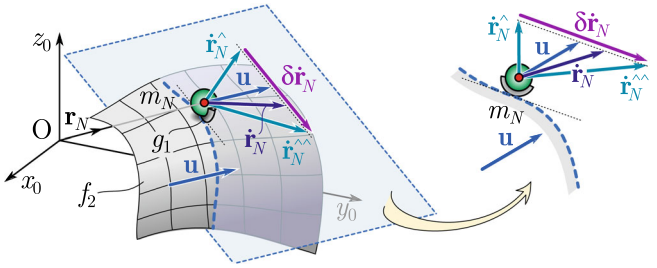

Fig. 23 Actual, admissible and virtual velocities. Skating on a non-stationary surface that translates with velocity $\mathbf{u}$. The virtual velocity is tangential to the surface

in Fig. 23. Notice that despite δ often refers to variations, the virtual velocities are not infinitesimal quantities.

Using the definitions above, one may reformulate (148) as follows. Since the admissible velocities satisfy the constraints (148), the velocities $\dot{\mathbf{r}}_i^{\wedge}$ and $\dot{\mathbf{r}}_i^{\wedge\wedge}$ may be substituted there instead of $\dot{\mathbf{r}}_i$. Then taking the difference of the two leads to

$$\sum_{i=1}^{N} \mathbf{w}_{\beta i}(\mathbf{r}_j, t) \cdot \delta\dot{\mathbf{r}}_i = 0, \quad \beta = 1, \ldots, h \tag{149}$$

that are linear in the virtual velocities $\delta\dot{\mathbf{r}}_i$.

The power of the force $\mathbf{F}_i$ acting on particle i is defined as $P_i = \mathbf{F}_i \cdot \dot{\mathbf{r}}_i$. Based on the definitions above, the virtual power can also be defined as $\delta P_i = \mathbf{F}_i \cdot \delta\dot{\mathbf{r}}_i$. Then, the ideal constraints are defined by requiring the virtual power of the corresponding constraining forces $\mathbf{K}_i$ to be zero:

$$\sum_{i=1}^{N} \mathbf{K}_i \cdot \delta\dot{\mathbf{r}}_i = 0. \tag{150}$$

Here we only consider ideal constraints, and the forces that do not satisfy (150) are called active forces and denoted by $\mathbf{F}_i$.

Thus, Newton's 2nd Law can be written in the form

$$m_i\ddot{\mathbf{r}}_i = \mathbf{F}_i + \mathbf{K}_i, \quad i = 1, \ldots, N, \tag{151}$$

where the active and the constraining forces are separated. By multiplying this equation with the corresponding virtual velocity $\delta\dot{\mathbf{r}}_i$, and summing for all particles, we obtain Jourdain's principle

$$\sum_{i=1}^{N} (m_i\ddot{\mathbf{r}}_i - \mathbf{F}_i) \cdot \delta\dot{\mathbf{r}}_i = 0, \tag{152}$$

where (150) is utilized. Similar result is obtained by applying D'Alembert's principle with virtual displacements instead of virtual velocities, which is widely used in statics (De Sapio, 2017). However, since virtual displacements are infinitesimal quantities, it is challenging to use them in dynamical problems (Antman, 1992).

6.2 Generalized Coordinates and Pseudo Velocities

To eliminate the g geometric constraints (146) and the corresponding geometric constraining forces from the governing equations, one needs to select $3N - g$ so-called generalized coordinates $q_k, k = 1, \ldots, 3N - g$ intuitively. The chosen definitions

$$q_k := H_k(\mathbf{r}_i, t)\,, \quad k = 1, \ldots, 3N - g \tag{153}$$

can be considered appropriate if these generalized coordinates, together with the geometric constraints (146), provide an unambiguous description of the dynamical system. In mathematical terms, this means that the system (146), (153), which consists of $3N$ nonlinear algebraic equations, has a unique solution for the $3N$ unknown coordinates of the position vectors $\mathbf{r}_i\,,\ i = 1, \ldots, N$. Consequently, if the generalized coordinate selection is appropriate, a unique solution

$$\mathbf{r}_i(q_k, t)\,, \quad i = 1, \ldots, N \tag{154}$$

exists, where again, we use the abbreviated notation that q_k represents $q_1, \ldots, q_{3N-g}$. We remark that the explicit time dependence of (153) and (154) originates in the fact that, in general, the constraints (146), (147) and (148) can be time dependent.

Taking the time derivative of (154) allows us to express the velocities $\dot{\mathbf{r}}_i$ as an affine function of the generalized velocities $\dot{q}_k$:

$$\dot{\mathbf{r}}_i = \sum_{k=1}^{3N-g} \frac{\partial \mathbf{r}_i(q_\ell, t)}{\partial q_k} \dot{q}_k + \frac{\partial \mathbf{r}_i(q_\ell, t)}{\partial t}, \quad i = 1, \ldots, N. \tag{155}$$

Similarly to (148) and (149), this can be rewritten for the virtual velocities $\delta\dot{\mathbf{r}}_i = \dot{\mathbf{r}}_i^{\wedge} - \dot{\mathbf{r}}_i^{\wedge\wedge}$ by means of the virtual generalized velocities $\delta\dot{q}_k = \dot{q}_k^{\wedge} - \dot{q}_k^{\wedge\wedge}$ as

$$\delta\dot{\mathbf{r}}_i = \sum_{k=1}^{3N-g} \frac{\partial \mathbf{r}_i(q_\ell, t)}{\partial q_k} \delta\dot{q}_k, \quad i = 1, \ldots, N\,. \tag{156}$$

Substituting (155) into (148) yields the kinematic constraints in the form

$$\sum_{k=1}^{3N-g} A_{\beta k}(q_\ell, t)\, \dot{q}_k + A_\beta(q_\ell, t) = 0, \quad \beta = 1, \ldots, h \tag{157}$$

that are expressed with respect to the generalized velocities as

$$\begin{aligned} A_{\beta k}(q_\ell, t) &= \sum_{i=1}^{N} \mathbf{w}_{\beta i}\big(\mathbf{r}_j(q_\ell, t), t\big) \cdot \frac{\partial \mathbf{r}_i(q_\ell, t)}{\partial q_k}, \\ A_\beta(q_\ell, t) &= \sum_{i=1}^{N} \mathbf{w}_{\beta i}\big(\mathbf{r}_j(q_\ell, t), t\big) \cdot \frac{\partial \mathbf{r}_i(q_\ell, t)}{\partial t} + w_\beta\big(\mathbf{r}_j(q_\ell, t), t\big). \end{aligned} \tag{158}$$

Substituting (156) into (149) yields the kinematic constraints in the form

$$\sum_{k=1}^{3N-g} A_{\beta k}(q_\ell, t)\, \delta\dot{q}_k = 0, \quad \beta = 1, \ldots, h, \tag{159}$$

expressed with the virtual generalized velocities.

One may derive the equations of motion in terms of the generalized coordinates q_k by substituting (156) into Jourdain's principle (152). This results in the Lagrange equations of the second kind for nonholonomic systems. However, this approach requires the use of Lagrange multipliers and leads to algebraic differential equations; see Routh (1884), Voss (1885). Here we chose a different approach which results in ordinary differential equations; see Appell (1900), Gibbs (1879).

To eliminate the kinematic (nonholonomic) constraints, one needs to select $n = 3N - g - h$ so-called pseudo velocities σ_j, $j = 1, \ldots, n$ intuitively. These have to be defined appropriately as the linear combinations of the generalized velocities $\dot{q}_k$, $k = 1, \ldots, 3N - g$, such that

$$\sigma_j := \sum_{k=1}^{3N-g} B_{jk}(q_\ell, t)\, \dot{q}_k, \quad j = 1, \ldots, n. \tag{160}$$

Similarly to the requirements for the selection of the generalized coordinates in (153), the functions B_{jk} must be selected in a way that the defined pseudo velocities σ_j provide an unambiguous description of the system dynamics. Accordingly, the definitions of the pseudo velocities (160) together with the kinematic constraints (157) constitute a $(3N - g)$-dimensional system of linear algebraic equations with respect to the generalized velocities. This can be written in the form

$$\underbrace{\begin{bmatrix} A_{11} & \dots & A_{1(3N-g)} \\ \vdots & \ddots & \vdots \\ A_{h1} & \dots & A_{h(3N-g)} \\ B_{11} & \dots & B_{1(3N-g)} \\ \vdots & \ddots & \vdots \\ B_{n1} & \dots & B_{n(3N-g)} \end{bmatrix}}_{=:\mathbf{C}} \begin{bmatrix} \dot{q}_1 \\ \vdots \\ \dot{q}_{3N-g} \end{bmatrix} = \begin{bmatrix} -A_1 \\ \vdots \\ -A_h \\ \sigma_1 \\ \vdots \\ \sigma_n \end{bmatrix}, \tag{161}$$

which has a unique solution for the generalized velocities $\dot{q}_k$ if the coefficient matrix $\mathbf{C}$ is not singular in the configuration space of the generalized coordinates q_ℓ at any time:

$$\det\big(\mathbf{C}(q_\ell, t)\big) \neq 0. \tag{162}$$

Then the generalized velocities can be expressed as a unique function of the pseudo velocities, generalized coordinates and time:

$$\dot{q}_k = \sum_{j=1}^{n} f_{kj}(q_\ell, t)\, \sigma_j + f_k(q_\ell, t), \quad k = 1, \dots, 3N - g, \tag{163}$$

similarly to the generalized coordinates expressed as unique functions of the system position vectors in (154).

6.3 Appell–Gibbs Equations

Substituting (163) into (155), we can express the velocities with the pseudo velocities as

$$\dot{\mathbf{r}}_i = \sum_{j=1}^{n} \mathbf{d}_{ij}(q_\ell, t)\, \sigma_j + \mathbf{d}_i(q_\ell, t), \quad i = 1, \dots, N, \tag{164}$$

where

$$\begin{aligned} \mathbf{d}_{ij}(q_\ell, t) &= \sum_{k=1}^{3N-g} \frac{\partial \mathbf{r}_i(q_\ell, t)}{\partial q_k} f_{kj}(q_\ell, t), \\ \mathbf{d}_i(q_\ell, t) &= \sum_{k=1}^{3N-g} \frac{\partial \mathbf{r}_i(q_\ell, t)}{\partial q_k} f_k(q_\ell, t) + \frac{\partial \mathbf{r}_i(q_\ell, t)}{\partial t}. \end{aligned} \tag{165}$$

Similarly to (148) and (149), formula (164) can be rewritten for the virtual velocities $\delta\dot{\mathbf{r}}_i = \dot{\mathbf{r}}_i^{\wedge} - \dot{\mathbf{r}}_i^{\wedge\wedge}$ using the virtual pseudo velocities $\delta\sigma_j = \sigma_j^{\wedge} - \sigma_j^{\wedge\wedge}$:

$$\delta\dot{\mathbf{r}}_i = \sum_{j=1}^{n} \mathbf{d}_{ij}(q_\ell, t)\, \delta\sigma_j, \quad i = 1, \ldots, N\,, \tag{166}$$

cf. the derivation of (156) from (155).

Also, differentiating (164) yields the acceleration

$$\ddot{\mathbf{r}}_i = \sum_{j=1}^{n} \mathbf{d}_{ij}(q_\ell, t)\, \dot{\sigma}_j + \ldots, \quad i = 1, \ldots, N\,, \tag{167}$$

where ... represent terms that contain only generalized coordinates q_ℓ, pseudo velocities σ_j, and time t, but do not contain pseudo accelerations $\dot{\sigma}_j$. Observe that (167) results in

$$\frac{\partial \ddot{\mathbf{r}}_i}{\partial \dot{\sigma}_j} = \mathbf{d}_{ij}(q_\ell, t). \tag{168}$$

Recall Jourdain's principle in (152), where the substitution of (166) leads to

$$\sum_{j=1}^{n} \left(\sum_{i=1}^{N} m_i \ddot{\mathbf{r}}_i \cdot \mathbf{d}_{ij} - \sum_{i=1}^{N} \mathbf{F}_i \cdot \mathbf{d}_{ij} \right) \delta\sigma_j = 0. \tag{169}$$

Using (168) and the chain rule, one can reformulate (169) as

$$\sum_{j=1}^{n} \left(\frac{\partial S}{\partial \dot{\sigma}_j} - \Pi_j \right) \delta\sigma_j = 0, \tag{170}$$

where

$$S = \frac{1}{2} \sum_{i=1}^{N} m_i\, \ddot{\mathbf{r}}_i^2, \tag{171}$$

is the so-called acceleration energy (or Gibbs function) of the system, and the pseudo force Π_j is defined by

$$\Pi_j = \sum_{i=1}^{N} \mathbf{F}_i \cdot \mathbf{d}_{ij}, \quad j = 1, \ldots, n. \tag{172}$$

Since the virtual pseudo velocities $\delta\sigma_j$ in (170) are not constrained, the parentheses can be equated to zero yielding the Appell–Gibbs equations

$$\frac{\partial S}{\partial \dot{\sigma}_j} = \Pi_j, \qquad j = 1, \ldots, n. \tag{173}$$

These, together with (163), constitute the equations of motion

$$\begin{aligned} \frac{\partial S}{\partial \dot{\sigma}_j} &= \Pi_j, \qquad\qquad j = 1, \ldots, n, \\ \dot{q}_k &= \sum_{j=1}^{n} f_{kj}\sigma_j + f_k, \quad k = 1, \ldots, 3N - g, \end{aligned} \tag{174}$$

which is a system of $n + 3N - g = 6N - 2g - h$ first-order ordinary differential equations for the $n = 3N - g - h$ pseudo velocities σ_j and the $3N - g$ generalized coordinates q_k, corresponding to the $3N - g - h/2$ degrees of freedom of the system.

The pseudo forces (172) may be calculated by noticing that the virtual power of the active forces is the same as that of the pseudo forces, that is, using (166) we obtain

$$\delta P = \sum_{i=1}^{N} \mathbf{F}_i \cdot \delta \dot{\mathbf{r}}_i = \sum_{j=1}^{n} \sum_{i=1}^{N} \mathbf{F}_i \cdot \mathbf{d}_{ij}\, \delta\sigma_j = \sum_{j=1}^{n} \Pi_j \delta\sigma_j. \tag{175}$$

6.4 Extension to Rigid Bodies

When the theory is applied for multi-body systems, the acceleration energy of each rigid body has to be calculated as

$$S = \frac{1}{2} \int_{(m)} \mathbf{a}^2 \, \mathrm{d}m \,, \tag{176}$$

where $\mathbf{a} \equiv \ddot{\mathbf{r}}$ refers to the acceleration of a particle of the rigid body; see Fig. 24. Based on the rigid body kinematics, the acceleration of any particle can be calculated as

$$\mathbf{a} = \mathbf{a}_\mathrm{G} + \boldsymbol{\alpha} \times \boldsymbol{\rho} + \boldsymbol{\omega} \times (\boldsymbol{\omega} \times \boldsymbol{\rho}), \tag{177}$$

where $\mathbf{a}_\mathrm{G}$ is the acceleration of the center of mass G, $\boldsymbol{\alpha}$ and $\boldsymbol{\omega}$ are the angular acceleration and angular velocity vectors of the body, respectively. Thus,

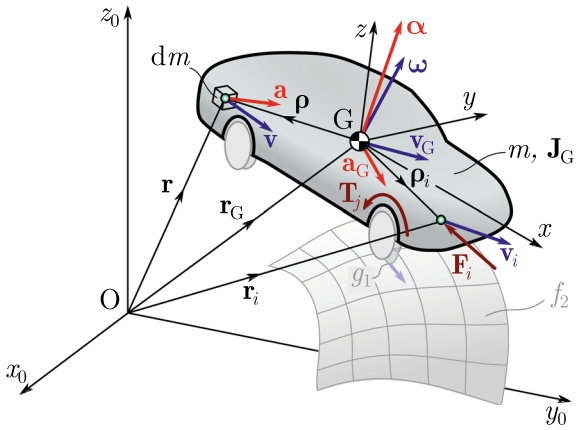

Fig. 24 Derivation of the acceleration energy for rigid bodies and the virtual power of active forces acting on rigid bodies

$$
\begin{aligned}
S =& \frac{1}{2}\int_{(m)} (\mathbf{a}_\mathrm{G} + \boldsymbol{\alpha}\times\boldsymbol{\rho} + \boldsymbol{\omega}\times(\boldsymbol{\omega}\times\boldsymbol{\rho}))^2 \,\mathrm{d}m \\
=& \frac{1}{2}\int_{(m)} \mathbf{a}_\mathrm{G}^2 \,\mathrm{d}m + \frac{1}{2}\int_{(m)} \underbrace{(\boldsymbol{\alpha}\times\boldsymbol{\rho})\cdot(\boldsymbol{\alpha}\times\boldsymbol{\rho})}_{=\boldsymbol{\alpha}\cdot(\boldsymbol{\rho}\times(\boldsymbol{\alpha}\times\boldsymbol{\rho}))} \,\mathrm{d}m \\
&+ \int_{(m)} \mathbf{a}_\mathrm{G}\cdot(\boldsymbol{\alpha}\times\boldsymbol{\rho})\,\mathrm{d}m + \int_{(m)} \mathbf{a}_\mathrm{G}\cdot(\boldsymbol{\omega}\times(\boldsymbol{\omega}\times\boldsymbol{\rho}))\,\mathrm{d}m \\
&+ \int_{(m)} \underbrace{(\boldsymbol{\alpha}\times\boldsymbol{\rho})\cdot(\boldsymbol{\omega}\times(\boldsymbol{\omega}\times\boldsymbol{\rho}))}_{=\boldsymbol{\alpha}\cdot(\boldsymbol{\rho}\times(\boldsymbol{\omega}\times(\boldsymbol{\omega}\times\boldsymbol{\rho})))} \,\mathrm{d}m \\
&+ \frac{1}{2}\int_{(m)} \underbrace{(\boldsymbol{\omega}\times(\boldsymbol{\omega}\times\boldsymbol{\rho}))^2}_{\text{does not depend on } \dot{\sigma}_j} \,\mathrm{d}m \\
=& \underbrace{\frac{1}{2}\int_{(m)} 1\,\mathrm{d}m}_{=m}\,\mathbf{a}_\mathrm{G}^2 + \frac{1}{2}\boldsymbol{\alpha}\cdot\underbrace{\int_{(m)} (\boldsymbol{\rho}^2\mathbf{I} - \boldsymbol{\rho}\otimes\boldsymbol{\rho})\,\mathrm{d}m}_{=\mathbf{J}_\mathrm{G}}\,\boldsymbol{\alpha} \\
&+ \mathbf{a}_\mathrm{G}\cdot\Bigg(\boldsymbol{\alpha}\times\underbrace{\int_{(m)}\boldsymbol{\rho}\,\mathrm{d}m}_{=\mathbf{0}}\Bigg) + \mathbf{a}_\mathrm{G}\cdot\Bigg(\boldsymbol{\omega}\times\Big(\boldsymbol{\omega}\times\underbrace{\int_{(m)}\boldsymbol{\rho}\,\mathrm{d}m}_{=\mathbf{0}}\Big)\Bigg) \\
&+ \boldsymbol{\alpha}\cdot\Bigg(\boldsymbol{\omega}\times\underbrace{\int_{(m)}(\boldsymbol{\rho}^2\mathbf{I} - \boldsymbol{\rho}\otimes\boldsymbol{\rho})\,\mathrm{d}m}_{=\mathbf{J}_\mathrm{G}}\,\boldsymbol{\omega}\Bigg) + \ldots\,,
\end{aligned}
\tag{178}
$$

where m is the mass of the body, $\otimes$ is the diadic product, and $\mathbf{J}_\mathrm{G}$ is the mass moment of inertia tensor about the center of mass G. There is no need to calculate the additional terms referred to by ... since they do not contain accelerations, and consequently, their derivatives are always zero with respect to the pseudo accelerations $\dot{\sigma}_j$ in the Appell-Gibbs equations (173).

Finally, the acceleration energy of a rigid body can be calculated as

$$S = \frac{1}{2} m \mathbf{a}_\mathrm{G}^2 + \frac{1}{2} \boldsymbol{\alpha} \cdot \mathbf{J}_\mathrm{G} \boldsymbol{\alpha} + \boldsymbol{\alpha} \cdot (\boldsymbol{\omega} \times \mathbf{J}_\mathrm{G} \boldsymbol{\omega}) + \ldots \tag{179}$$

where $\mathbf{H}_\mathrm{G} = \mathbf{J}_\mathrm{G} \boldsymbol{\omega}$ is the angular momentum vector about the center of mass G, that is, the last term is a triple product of the angular acceleration, the angular velocity, and the angular momentum vectors. In planar problems these vectors are parallel, i.e., $\boldsymbol{\alpha} \parallel \boldsymbol{\omega} \parallel \mathbf{H}_\mathrm{G}$, so the last term becomes zero. In the problems considered in this book chapter, this is indeed the case.

Moreover, the virtual power (175) of the active force system acting on the rigid body can be calculated by summing the virtual powers of each active force $\mathbf{F}_i$ that acts on the i-th particle of the rigid body. In addition, the torques $\mathbf{T}_j$ acting on the rigid body also have to be considered, namely:

$$\begin{aligned} \delta P &= \sum_i \mathbf{F}_i \cdot \delta \mathbf{v}_i + \sum_j \mathbf{T}_j \cdot \delta \boldsymbol{\omega} \\ &= \sum_i \mathbf{F}_i \cdot \delta (\mathbf{v}_\mathrm{G} + \boldsymbol{\omega} \times \boldsymbol{\rho}_i) + \sum_j \mathbf{T}_j \cdot \delta \boldsymbol{\omega} \\ &= \underbrace{\Big(\sum_i \mathbf{F}_i \Big)}_{=\mathbf{F}} \cdot \delta \mathbf{v}_\mathrm{G} + \underbrace{\Big(\sum_i \boldsymbol{\rho}_i \times \mathbf{F}_i + \sum_j \mathbf{T}_j \Big)}_{=\mathbf{M}_\mathrm{G}} \cdot \delta \boldsymbol{\omega} \,. \end{aligned} \tag{180}$$

That is, the virtual power can be calculated as

$$\delta P = \mathbf{F} \cdot \delta \mathbf{v}_\mathrm{G} + \mathbf{M}_\mathrm{G} \cdot \delta \boldsymbol{\omega}, \tag{181}$$

where $\mathbf{F}$ is the resultant force, while $\mathbf{M}_\mathrm{G}$ is the resultant torque about the center of mass G.

To calculate the right hand side of the Appell-Gibbs equations (173) in case of multi-body system, one can calculate the virtual power of the active forces acting on the rigid body using (181) and identify the pseudo forces via (175).

7 Deriving the Equation of Motion Using Point R

7.1 Without Steering Dynamics

The system (114), (115) can be solved for the generalized velocities:

$$\begin{aligned} \dot{x}_\mathrm{R} &= V\cos\psi - \hat{\sigma}\sin\psi, \\ \dot{y}_\mathrm{R} &= V\sin\psi + \hat{\sigma}\cos\psi, \\ \dot{\psi} &= \omega, \end{aligned} \tag{182}$$

and taking the time derivative yields

$$\begin{aligned} \ddot{x}_\mathrm{R} &= -V\omega\sin\psi - \dot{\hat{\sigma}}\sin\psi - \hat{\sigma}\omega\cos\psi, \\ \ddot{y}_\mathrm{R} &= V\omega\cos\psi + \dot{\hat{\sigma}}\cos\psi - \hat{\sigma}\omega\sin\psi, \\ \ddot{\psi} &= \dot{\omega}. \end{aligned} \tag{183}$$

Here $\ddot{x}_\mathrm{R}$ and $\ddot{y}_\mathrm{R}$ are the acceleration components of the rear axle center R in the Earth fixed frame $\mathcal{F}_0$, see (3).

In order to calculate the acceleration energy we still need the acceleration of the center of mass G:

$$\begin{aligned} \begin{bmatrix} \ddot{x}_\mathrm{G} \\ \ddot{y}_\mathrm{G} \end{bmatrix}_{\mathcal{F}_0} &= \begin{bmatrix} \ddot{x}_\mathrm{R} - d\,\ddot{\psi}\sin\psi - d\,\dot{\psi}^2\cos\psi \\ \ddot{y}_\mathrm{R} + d\,\ddot{\psi}\cos\psi - d\,\dot{\psi}^2\sin\psi \end{bmatrix}_{\mathcal{F}_0} \\ &= \begin{bmatrix} -V\omega\sin\psi - \dot{\hat{\sigma}}\sin\psi - \hat{\sigma}\omega\cos\psi - d\,\dot{\omega}\sin\psi - d\omega^2\cos\psi \\ V\omega\cos\psi + \dot{\hat{\sigma}}\cos\psi - \hat{\sigma}\omega\sin\psi + d\,\dot{\omega}\cos\psi - d\omega^2\sin\psi \end{bmatrix}_{\mathcal{F}_0}, \end{aligned} \tag{184}$$

where in the last step we substituted (183).

Then the acceleration energy of the system becomes

$$\begin{aligned} S &= \frac{1}{2}m\left(\ddot{x}_\mathrm{G}^2 + \ddot{y}_\mathrm{G}^2\right) + \frac{1}{2}J_\mathrm{G}\ddot{\psi}^2 + \ldots \\ &= \frac{1}{2}m\left(\dot{\hat{\sigma}}^2 + d^2\dot{\omega}^2 + 2V\omega\dot{\hat{\sigma}} + 2Vd\omega\dot{\omega} + 2d\dot{\hat{\sigma}}\dot{\omega}\right) + \frac{1}{2}J_\mathrm{G}\dot{\omega}^2 + \ldots, \end{aligned} \tag{185}$$

where the terms without $\dot{\hat{\sigma}}$ or $\dot{\omega}$ are incorporated in ....

The virtual power of the active forces $\mathbf{F}_\mathrm{R}$, $\mathbf{F}_\mathrm{F}$ and torques M_R, M_F is still given in the form

$$\delta P = \mathbf{F}_\mathrm{R}\cdot\delta\mathbf{v}_\mathrm{R} + \mathbf{F}_\mathrm{F}\cdot\delta\mathbf{v}_\mathrm{F} + (M_\mathrm{R} + M_\mathrm{F})\,\delta\omega, \tag{186}$$

but now the velocities of the point R and F are expressed as

$$\mathbf{v}_{\mathrm{R}} = \begin{bmatrix} V \\ \hat{\sigma} \end{bmatrix}_{\mathcal{F}_1}, \qquad \mathbf{v}_{\mathrm{F}} = \mathbf{v}_{\mathrm{R}} + \boldsymbol{\omega} \times \mathbf{r}_{\mathrm{RF}} = \begin{bmatrix} V \\ \hat{\sigma} + l\,\omega \end{bmatrix}_{\mathcal{F}_1}, \tag{187}$$

where we used the angular velocity $\boldsymbol{\omega} = \begin{bmatrix} 0 & 0 & \omega \end{bmatrix}_{\mathcal{F}_1}^{\top}$ and $\mathbf{r}_{\mathrm{RF}} = \begin{bmatrix} 0 & l & 0 \end{bmatrix}_{\mathcal{F}_1}^{\top}$. These result in the slip angles

$$\tan \alpha_{\mathrm{R}} = -\frac{v_{\mathrm{R}}^{y_1}}{v_{\mathrm{R}}^{x_1}} = -\frac{\hat{\sigma}}{V}, \qquad \tan\left(\alpha_{\mathrm{F}} - \gamma\right) = -\frac{v_{\mathrm{F}}^{y_1}}{v_{\mathrm{F}}^{x_1}} = -\frac{\hat{\sigma} + l\,\omega}{V}, \tag{188}$$

and substituting them into (186) together with the tire forces

$$\mathbf{F}_{\mathrm{R}} = \begin{bmatrix} 0 \\ F_{\mathrm{R}} \end{bmatrix}_{\mathcal{F}_1}, \qquad \mathbf{F}_{\mathrm{F}} = \begin{bmatrix} -F_{\mathrm{F}} \sin\gamma \\ F_{\mathrm{F}} \cos\gamma \end{bmatrix}_{\mathcal{F}_1}, \tag{189}$$

results in the virtual power

$$\begin{aligned} \delta P &= F_{\mathrm{R}}\,\delta\hat{\sigma} - F_{\mathrm{F}} \sin\gamma\,\delta V + F_{\mathrm{F}} \cos\gamma\,\delta\left(\hat{\sigma} + l\omega\right) + \left(M_{\mathrm{R}} + M_{\mathrm{F}}\right)\delta\omega \\ &= \left(F_{\mathrm{R}} + F_{\mathrm{F}} \cos\gamma\right)\delta\hat{\sigma} + \left(l\,F_{\mathrm{F}} \cos\gamma + M_{\mathrm{R}} + M_{\mathrm{F}}\right)\delta\omega, \end{aligned} \tag{190}$$

where we used that $\delta V = 0$. The coefficients of the virtual pseudo velocities $\delta\hat{\sigma}$ and $\delta\omega$ lead to the the pseudo forces

$$\begin{aligned} \Pi_{\hat{\sigma}} &= F_{\mathrm{R}} + F_{\mathrm{F}} \cos\gamma, \\ \Pi_{\omega} &= l\,F_{\mathrm{F}} \cos\gamma + M_{\mathrm{R}} + M_{\mathrm{F}}. \end{aligned} \tag{191}$$

Then (185) and (191) yield the Appell equations

$$\begin{aligned} \frac{\partial S}{\partial \dot{\hat{\sigma}}} = \Pi_{\hat{\sigma}} \quad &\Rightarrow \quad m\left(\dot{\hat{\sigma}} + V\omega + d\,\dot{\omega}\right) = F_{\mathrm{R}} + F_{\mathrm{F}} \cos\gamma\,, \\ \frac{\partial S}{\partial \dot{\omega}} = \Pi_{\omega} \quad &\Rightarrow \quad md\left(\dot{\hat{\sigma}} + V\omega + d\,\dot{\omega}\right) + J_{\mathrm{G}}\dot{\omega} = l\,F_{\mathrm{F}} \cos\gamma + M_{\mathrm{R}} + M_{\mathrm{F}}. \end{aligned} \tag{192}$$

Combining these with the kinematic equations (182) gives the equations of motion

$$\begin{aligned} \begin{bmatrix} m & md \\ md & J_{\mathrm{G}} + md^2 \end{bmatrix}\begin{bmatrix} \dot{\hat{\sigma}} \\ \dot{\omega} \end{bmatrix} + \begin{bmatrix} mV\omega \\ mdV\omega \end{bmatrix} &= \begin{bmatrix} F_{\mathrm{R}} + F_{\mathrm{F}} \cos\gamma \\ lF_{\mathrm{F}} \cos\gamma + M_{\mathrm{R}} + M_{\mathrm{F}} \end{bmatrix}, \\ \dot{\psi} &= \omega, \\ \dot{x}_{\mathrm{R}} &= V \cos\psi - \hat{\sigma} \sin\psi, \\ \dot{y}_{\mathrm{R}} &= V \sin\psi + \hat{\sigma} \cos\psi. \end{aligned} \tag{193}$$

Here the first equation still corresponds to the lateral dynamics while the second equation is a torque equation about the point R. However, the first two equations are

coupled in $\dot{\hat{\sigma}}$ and $\dot{\omega}$. These can be decoupled using some algebraic manipulations, yielding

$$
\begin{aligned}
m\left(\dot{\hat{\sigma}} + V\omega\right) &= \left(1 + \frac{md^2}{J_\mathrm{G}}\right) F_\mathrm{R} + \left(1 - \frac{md(l-d)}{J_\mathrm{G}}\right) F_\mathrm{F} \cos\gamma \\
&\quad - \frac{md}{J_\mathrm{G}} \left(M_\mathrm{R} + M_\mathrm{F}\right), \\
J_\mathrm{G}\dot{\omega} &= -d\, F_\mathrm{R} + (l-d) F_\mathrm{F} \cos\gamma + M_\mathrm{R} + M_\mathrm{F}, \\
\dot{\psi} &= \omega, \\
\dot{x}_\mathrm{R} &= V\cos\psi - \hat{\sigma}\sin\psi, \\
\dot{y}_\mathrm{R} &= V\sin\psi + \hat{\sigma}\cos\psi,
\end{aligned}
\tag{194}
$$

where the second equation is the torque equation about point G as in (113).

7.2 With Steering Dynamics

When the steering dynamics is added, the system (114), (115), (134) can be solved for the generalized velocities

$$
\begin{aligned}
\dot{x}_\mathrm{R} &= V\cos\psi - \hat{\sigma}\sin\psi, \\
\dot{y}_\mathrm{R} &= V\sin\psi + \hat{\sigma}\cos\psi, \\
\dot{\psi} &= \omega, \\
\dot{\gamma} &= \Omega,
\end{aligned}
\tag{195}
$$

whose time derivative is

$$
\begin{aligned}
\ddot{x}_\mathrm{R} &= -V\omega\sin\psi - \dot{\hat{\sigma}}\sin\psi - \hat{\sigma}\omega\cos\psi, \\
\ddot{y}_\mathrm{R} &= V\omega\cos\psi + \dot{\hat{\sigma}}\cos\psi - \hat{\sigma}\omega\sin\psi, \\
\ddot{\psi} &= \dot{\omega}, \\
\ddot{\gamma} &= \dot{\Omega}.
\end{aligned}
\tag{196}
$$

Then, utilizing (184), the acceleration energy of the system becomes

$$
\begin{aligned}
S &= \frac{1}{2}m\left(\ddot{x}_\mathrm{G}^2 + \ddot{y}_\mathrm{G}^2\right) + \frac{1}{2}J_\mathrm{G}\ddot{\psi}^2 + \frac{1}{2}J_\mathrm{F}\left(\ddot{\psi} + \ddot{\gamma}\right)^2 + \cdots \\
&= \frac{1}{2}m\left(\dot{\hat{\sigma}}^2 + d^2\dot{\omega}^2 + 2V\omega\dot{\hat{\sigma}} + 2Vd\omega\dot{\omega} + 2d\dot{\hat{\sigma}}\dot{\omega}\right) + \frac{1}{2}J_\mathrm{G}\dot{\omega}^2 \\
&\quad + \frac{1}{2}J_\mathrm{F}\left(\dot{\omega} + \dot{\Omega}\right)^2 + \cdots,
\end{aligned}
\tag{197}
$$

where, again, the terms without $\dot{\hat{\sigma}}$, $\dot{\omega}$ or $\dot{\Omega}$ are incorporated in ....

The virtual power of the active forces $\mathbf{F}_\mathrm{R}$, $\mathbf{F}_\mathrm{F}$ and torques M_R, M_F, T_s is given as

$$\delta P = (F_\mathrm{R} + F_\mathrm{F}\cos\gamma)\,\delta\hat{\sigma} + (l\,F_\mathrm{F}\cos\gamma + M_\mathrm{R} + M_\mathrm{F})\,\delta\omega + (M_\mathrm{F} + T_\mathrm{s})\,\delta\Omega, \tag{198}$$

where the coefficients of the virtual pseudo velocities $\delta\hat{\sigma}$, $\delta\omega$ and $\delta\Omega$ lead to the pseudo forces

$$\begin{aligned} \Pi_{\hat{\sigma}} &= F_\mathrm{R} + F_\mathrm{F}\cos\gamma, \\ \Pi_{\omega} &= l\,F_\mathrm{F}\cos\gamma + M_\mathrm{R} + M_\mathrm{F}, \\ \Pi_{\Omega} &= M_\mathrm{F} + T_\mathrm{s}. \end{aligned} \tag{199}$$

Then (197) and (199) yield the Appell equations

$$\begin{aligned} \frac{\partial S}{\partial \dot{\hat{\sigma}}} = \Pi_{\hat{\sigma}} \quad &\Rightarrow \quad m\left(\dot{\hat{\sigma}} + V\omega + d\,\dot{\omega}\right) = F_\mathrm{R} + F_\mathrm{F}\cos\gamma\,, \\ \frac{\partial S}{\partial \dot{\omega}} = \Pi_{\omega} \quad &\Rightarrow \quad md\left(\dot{\hat{\sigma}} + V\omega + d\,\dot{\omega}\right) + J_\mathrm{G}\dot{\omega} + J_\mathrm{F}\left(\dot{\omega} + \dot{\Omega}\right) \\ &= \quad l\,F_\mathrm{F}\cos\gamma + M_\mathrm{R} + M_\mathrm{F}, \\ \frac{\partial S}{\partial \dot{\Omega}} = \Pi_{\Omega} \quad &\Rightarrow \quad J_\mathrm{F}\left(\dot{\omega} + \dot{\Omega}\right) = M_\mathrm{F} + T_\mathrm{s}. \end{aligned} \tag{200}$$

Combining these with the kinematic equations (195) yields the equation of motion

$$\begin{bmatrix} m & md & 0 \\ md & J_\mathrm{G} + md^2 + J_\mathrm{F} & J_\mathrm{F} \\ 0 & J_\mathrm{F} & J_\mathrm{F} \end{bmatrix} \begin{bmatrix} \dot{\hat{\sigma}} \\ \dot{\omega} \\ \dot{\Omega} \end{bmatrix} + \begin{bmatrix} mV\omega \\ mdV\omega \\ 0 \end{bmatrix} = \begin{bmatrix} F_\mathrm{R} + F_\mathrm{F}\cos\gamma \\ l\,F_\mathrm{F}\cos\gamma + M_\mathrm{R} + M_\mathrm{F} \\ M_\mathrm{F} + T_\mathrm{s} \end{bmatrix},$$

$$\begin{aligned} \dot{\gamma} &= \Omega, \\ \dot{\psi} &= \omega, \\ \dot{x}_\mathrm{R} &= V\cos\psi - \hat{\sigma}\sin\psi, \\ \dot{y}_\mathrm{R} &= V\sin\psi + \hat{\sigma}\cos\psi. \end{aligned} \tag{201}$$

The first three equations are coupled in $\dot{\hat{\sigma}}$, $\dot{\omega}$ and $\dot{\Omega}$. These can be decoupled using some algebraic manipulations to obtain

$$
\begin{aligned}
m\left(\dot{\hat{\sigma}}+V\omega\right) &= \left(1+\frac{md^2}{J_\mathrm{G}}\right)F_\mathrm{R}+\left(1-\frac{md(l-d)}{J_\mathrm{G}}\right)F_\mathrm{F}\cos\gamma \\
&\quad -\frac{md}{J_\mathrm{G}}\left(M_\mathrm{R}-T_\mathrm{s}\right), \\
J_\mathrm{G}\dot{\omega} &= -d\,F_\mathrm{R}+(l-d)F_\mathrm{F}\cos\gamma+M_\mathrm{R}-T_\mathrm{s}, \qquad (202)\\
J_\mathrm{F}\dot{\Omega} &= M_\mathrm{F}+T_\mathrm{s}-\frac{J_\mathrm{F}}{J_\mathrm{G}}\left(-d\,F_\mathrm{R}+(l-d)F_\mathrm{F}\cos\gamma+M_\mathrm{R}-T_\mathrm{s}\right), \\
\dot{\gamma} &= \Omega, \\
\dot{\psi} &= \omega, \\
\dot{x}_\mathrm{R} &= V\cos\psi-\hat{\sigma}\sin\psi, \\
\dot{y}_\mathrm{R} &= V\sin\psi+\hat{\sigma}\cos\psi,
\end{aligned}
$$

where the second and third equations are the same as those in (141). Also, one may observe that the first equation is almost the same as the first equation in (194), except that here $-T_\mathrm{s}$ shows up instead of M_F.

References

Antman, S. S. (1992). Mechanics: from Newton's laws to deterministic chaos. *SIAM Review, 34*(1), 135–137.

Appell, P. (1900). Sur une forme générale des équations de la dynamique (on a general form of the equations of dynamics). *Journal für die reine und angewandte Mathematik (Journal for Pure and Applied Mathematics), 121*, 310–319.

Baruh, H. (1999). *Analytical dynamics*. McGraw-Hill.

Beregi, S., Avedisov, S. S., He, C. R., Takács, D., & Orosz, G. (2023). Connectivity-based delay-tolerant control of automated vehicles: Theory and experiments. *IEEE Transactions on Intelligent Vehicles, 8*(1), 275–289.

Beregi, S., Takács, D., & Stépán, G. (2016). Tyre induced vibrations of the car-trailer system. *Journal of Sound and Vibration, 362*, 214–227.

Beregi, S., Takács, D., & Stépán, G. (2019). Bifurcation analysis of wheel shimmy with non-smooth effects and time delay in the tyre-ground contact. *Nonlinear Dynamics, 98*(1), 841–858.

Bloch, A. M. (2003). *Nonholonomic mechanics and control*. Springer.

De Sapio, V. (2017). *Advanced analytical dynamics: Theory and applications*. Cambridge: Cambridge University Press.

De Luca, A., Oriolo, G., & Samson, C. (1998). Feedback control of a nonholonomic car-like robot. In J.-P. Laumond (Ed.) *Robot motion planning and control* (pp. 171–249). Springer.

Euler, L. (1736). *Mechanica sive motus scientia analytice exposita (mechanics or motion science analytically exposed)*. Academy of Sciences.

Fiala, E. (1954). Seitenkräfte am rollenden Luftreifen (Lateral forces on the rolling pneumatic tire). *Zeitschrift der Vereines Deutscher Ingenieure (Magazine of the Association of German Engineers), 96*, 973–979.

Gantmacher, F. (1970). *Lectures in analytical mechanics*. Moscow: MIR Publishers.

Gibbs, J. W. (1879). On the fundamental formulae of dynamics. *American Journal of Mathematics, 2*(1), 49–64.

Gillespie, T. D. (1992). *Fundamentals of vehicle dynamics*. SAE International.

Goh, J. Y. M., Goel, T., & Gerdes, J. C. (2020). Toward automated vehicle control beyond the stability limits: Drifting along a general path. *Journal on Dynamic Systems Measurement and Control, 142*(2), 021004.

Goh, J. Y. M., Thompson, M., Dallas, J., & Balachandran, A. (2024). Beyond the stable handling limits: Nonlinear model predictive control for highly transient autonomous drifting. *Vehicle System Dynamics, 62*(10), 2590–2613.

Greenwood, D. T. (2003). *Adavanced dynamics*. Cambridge Univerisity Press.

Hamel, G. (1938). Nichtholonome Systeme höherer Art (Nonholonomic systems of a higher kind). *Sitzungsberichte der Berliner Mathematischen Gesellschaft (Meeting Reports of the Berlin Mathematical Society), 37*, 41–52.

Hu, H. (2018). On the degrees of freedom of a mechanical system. *Chinese Journal of Theoretical and Applied Mechanics, 50*(5), 1135–1144.

Kane, T. R., & Levinson, D. A. (1985). *Dynamics theory and applications*. McGraw-Hill.

Kane, T. R. (1961). Dynamics of nonholonomic systems. *ASME Journal on Applied Mechanics, 28*, 574–578.

Koon, W. S., & Marsden, J. E. (1997). The Hamiltonian and Lagrangian approaches to the dynamics of nonholonomic systems. *Reports on Mathematical Physics, 40*(1), 21–62.

Lagrange, J.-L. (1788). *Mécanique analytique (analytical mechanics)*. Ve Courcier, Paris.

Lenzo, B., Goel, T., & Gerdes, J. C. (2024). Autonomous drifting using torque vectoring: Innovating active safety. *IEEE Transactions on Intelligent Transportation Systems, 25*(11), 17931–17939.

Limebeer, D. J. N., & Massaro, M. (2018). *Dynamics and optimal control of road vehicles*. Oxford University Press.

Lu, H., Stépán, G., Lu, J., & Takács, D. (2022). Dynamics of vehicle stability control subjected to feedback delay. *European Journal of Mechanics A, 96*, 104678.

Mastinu, G., Della Rossa, F., Previati, G., Gobbi, M., & Fainello, M. (2023). Global stability of road vehicle motion with driver control. *Nonlinear Dynamics, 111*(19), 18043–18059.

Mi, T., Stépán, G., Takács, D., & Chen, N. (2020). Vehicle shimmy modeling with Pacejka's magic formula and the delayed tire model. *Journal on Computational Nonlinear Dynamics, 15*(3), 031005.

Neimark, J. I., & Fufaev, N. A. (1972). *Dynamics of nonholonomic systems, volume 33 of translations of mathematical monographs*. American Mathematical Society.

Newton, I. (1687). *Philosophiæ naturalis principia mathematica (mathematical principles of natural philosophy)*. Royal Society of London.

Oh, S., Avedisov, S. S., & Orosz, G. (2021). On the handling of automated vehicles: Modeling, bifurcation analysis, and experiments. *European Journal of Mechanics A, 90*, 104372.

Ostrovskaya, S., & Angeles, J. (1998). Nonholonomic systems revisited within the framework of analytical mechanics. *Applied Mechanics Reviews, 57*(7), 415–433.

Pacejka, H. B. (2002). *Tire and vehicle dynamics*. Oxford: Butterworth-Heinemann.

Papastavridis, J. G. (2002). *Analytical mechanics*. World Scientific.

Peterson, M. T., Goel, T., & Gerdes, J. C. (2023). Exploiting linear structure for precision control of highly nonlinear vehicle dynamics. *IEEE Transactions on Intelligent Vehicles, 8*(2), 1852–1862.

Popp, K., & Schiehlen, W. (2010). *Ground vehicle dynamics*. Springer.

Qin, W. B., Zhang, Y., Takács, D., Stépán, G., & Orosz, G. (2022). Nonholonomic dynamics and control of road vehicles: Moving toward automation. *Nonlinear Dynamics, 110*(3), 1959–2004.

Rajamani, R. (2012). *Vehicle dynamics and control*. Springer.

Routh, E. J. (1884). *The advanced part of a treatise on the dynamics of a system of rigid bodies*. MacMillan.

Schramm, D., Hiller, M., & Bardini, R. (2014). *Ground vehicle dynamics*. Springer.

Segel, L. (1956). Theoretical prediction and experimental substantiation of the response of the automobile to steering control. *Proceedings of the Institution of Mechanical Engineers: Automobile Division, 10*(1), 310–330.

Steindl, A., Edelmann, J., & Plöchl, M. (2023). Influence of tyre characteristics on periodic motions for an understeering vehicle. *PAMM, 22*(1), e202200289.

Takács, D., & Stépán, G. (2013). Contact patch memory of tyres leading to lateral vibrations of four-wheeled vehicles. *Philosophical Transactions of the Royal Society A, 371*(1993), 20120427.

Ulsoy, A. G., Peng, H., & Cakmakci, M. (2012). *Automotive control systems*. Cambridge University Press.

Várszegi, B., Takács, D., & Orosz, G. (2019). On the nonlinear dynamics of automated vehicles: A nonholonomic approach. *European Journal of Mechanics A, 74*, 371–380.

Voronets, P. V. (1901). Об уравненяках движеня для неголономных систем (On the equations of motion of nonholonomic systems). Математический Сборник*(Mathematical Collection), 22*(4), 659–686.

Vörös, I., & Takács, D. (2022). Lane-keeping control of automated vehicles with feedback delay: Nonlinear analysis and laboratory experiments. *European Journal of Mechanics A, 93*, 104509.

Vörös, I., Orosz, G., & Takács, D. (2023a). On the global dynamics of path-following control of automated passenger vehicles. *Nonlinear Dynamics, 111*(9), 8235–8252.

Vörös, I., Takács, D., & Orosz, G. (2023b). Safe lane-keeping with feedback delay: Bifurcation analysis and experiments. *IEEE Control Systems Letters, 7*, 1147–1152.

Voss, A. (1885). Ueber die Differentialgleichungen der Mechanik (About the differential equations of mechanics). *Mathematische Annalen (Mathematical Annals), 25*, 258–286.

Weber, T. P., & Gerdes, J. C. (2024). Modeling and control for dynamic drifting trajectories. *IEEE Transactions on Intelligent Vehicles, 9*(2), 3731–3741.